

## Synthesis, Activity, and Molecular Modeling Studies of Novel Human Aldose Reductase Inhibitors Based on a Marine Natural Product

Jesús Ángel de la Fuente,<sup>\*,†</sup> Sonia Manzanaro,<sup>†</sup> María Jesús Martín,<sup>‡</sup> Teresa G. de Quesada,<sup>‡</sup> Isabel Reymundo,<sup>‡</sup> Santos M. Luengo,<sup>§</sup> and Federico Gago<sup>§</sup>

Instituto Biomar, S.A., Polígono Industrial, Edificio CEEI, 24231 Onzonilla, León, Spain; Pharma Mar, S.A., Pol. Ind. La Mina-Norte, Avda. de los Reyes 1, 28770 Colmenar Viejo, Madrid, Spain; and Departamento de Farmacología, Universidad de Alcalá, 28871 Alcalá de Henares, Madrid, Spain

Received July 11, 2003

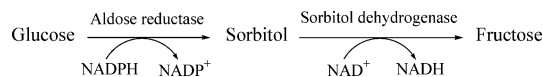
Aldose reductase (ALR2) has been implicated in the etiology of diabetic complications, including blindness. Because of the limited number of currently available drugs for the prevention of these long-term complications, the discovery of new ALR2 inhibitors appears highly desirable. In this study, a polybrominated diphenyl ether (**1**) naturally occurring in a marine sponge was found to inhibit recombinant human ALR2 with an  $IC_{50}$  of 6.4  $\mu$ M. A series of polyhalogenated analogues that were synthesized and tested in vitro to explore the structure–activity relationships displayed various degrees of inhibitory activity. The most active compounds were also capable of preventing sorbitol accumulation inside human retinal cells. In this cell-based assay, the most potent synthesized analogue (**16**) showed a 17-fold increase in inhibitory activity compared to that of sorbinil ( $IC_{50} = 0.24$  vs 4  $\mu$ M). A molecular representation of human ALR2 in complex with the natural product was built using homology modeling, automated docking, and energy refinement methods. AMBER parameters for the halogen atoms were derived and calibrated using condensed phase molecular dynamics simulations of fluorobenzene, chlorobenzene, and bromobenzene. Inhibitor binding is proposed to cause a conformational change similar to that recently reported for zenarestat. A free energy perturbation thermodynamic cycle allowed us to assess the importance of a crucial bromine atom that distinguishes the active lead compound from a much less active close natural analogue. Remarkably, the spatial location of this bromine atom is equivalent to that occupied by the only bromine atom present in zenarestat.

### Introduction

The elevated blood glucose levels that are characteristic of diabetes mellitus are responsible for the development of microvascular pathology in the retina, renal glomerulus, and peripheral nerve that can lead to blindness, renal failure, neuropathies, and cardiovascular disease. Among the mechanisms responsible for these complications, three appear to play a prominent role: (i) increased advanced glycation end-product formation, (ii) activation of protein kinase C isoforms, and (iii) increased flux of glucose through both the polyol and the hexosamine pathways. An integrating paradigm postulates a single hyperglycaemia-induced process of overproduction of superoxide by the mitochondrial electron-transport chain.<sup>1</sup>

The accumulated evidence supporting the importance of hyperglycemia-induced polyol pathway hyperactivity has led to a special focus on aldose reductase (alditol/NADP<sup>+</sup> oxidoreductase, EC1.1.1.21, ALR2) as a suitable target for pharmacological intervention.<sup>2–6</sup> This enzyme catalyzes the reduction of the aldehyde form of D-glucose to D-sorbitol with concomitant conversion of NADPH to NADP<sup>+</sup> (Scheme 1).<sup>7</sup> ALR2 inhibitors (ARIs) offer the possibility of preventing or arresting the progression of these long-term diabetic complications even in the

### Scheme 1. Polyol Pathway



presence of elevated blood glucose levels. Besides, since they have no effect on plasma glucose there is no associated risk of hypoglycemia.<sup>8</sup>

A large variety of structurally diverse compounds have been identified to date as potent in vitro ARIs.<sup>5,9–11</sup> The most potent and better characterized orally active ARIs belong to two main chemical classes: (i) carboxylic acid derivatives, such as tolrestat, zopolrestat, and zenarestat, and (ii) spiro-hydantoin, such as sorbinil (Figure 1).

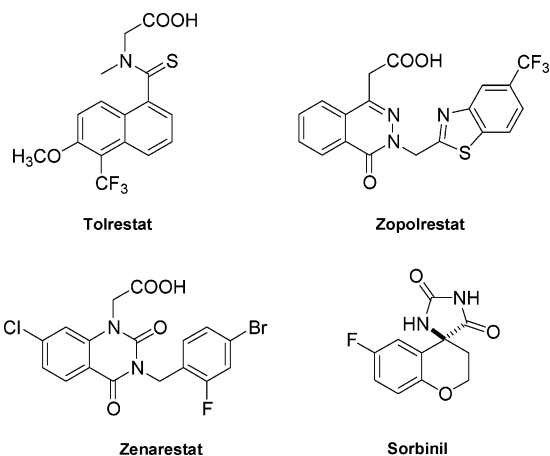
X-ray crystallographic studies on both porcine<sup>12,13</sup> and human<sup>14,15</sup> ALR2 (Figure 2) have shown that it belongs to the  $(\beta/\alpha)_8$ -barrel class of enzymes and that the coenzyme NAD(P) molecule binds at the C-terminal end of the  $\beta$  barrel. The large active site pocket is heavily lined with hydrophobic residues, which is consistent with the steroid dehydrogenase activity that is concomitantly associated with this enzyme<sup>16</sup> and also with the fact that glucose is an extremely poor substrate. In fact, currently known ARIs generally make use of both polar and nonpolar interactions to find complementarity with the extended enzyme binding pocket, which is best described as comprising two regions: (i) a polar site with residues Trp-20, Tyr-48 (the proton donor),<sup>17</sup> and His-110 and the positively charged nicotinamide moiety of NADP<sup>+</sup>, which accommodates the anionic carboxylate

\* To whom correspondence should be addressed. Telephone: +34–918466060. Fax: +34–918466001. E-mail: jdelafuente@pharmamar.com.

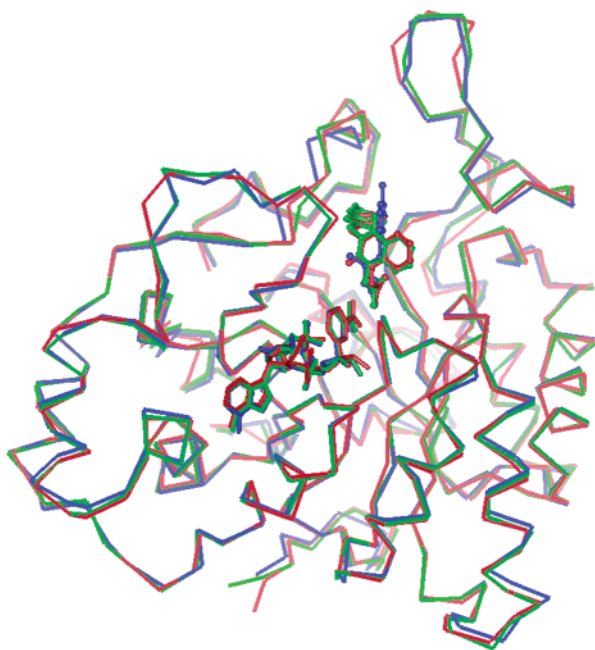
<sup>†</sup> Instituto Biomar, S.A.

<sup>‡</sup> Pharmamar, S.A.

<sup>§</sup> Universidad de Alcalá.



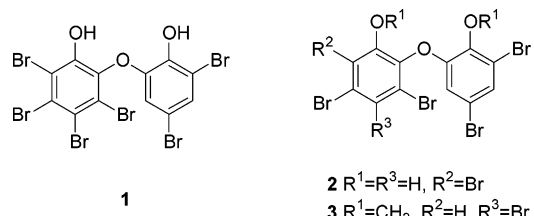
**Figure 1.** Some orally active ALR2 inhibitors.



**Figure 2.** View of superimposed C(α) traces of porcine ALR2 in complex with NADP and tolrestat (blue), human ALR2 in complex with NADP and zopolrestat (red), and human ALR2 in complex with NADP and zenarestat (green). NADP is shown as sticks, and the inhibitors are shown as balls and sticks.

or the ionizable hydantoin group of the ARI, and (ii) a nonpolar site with residues Trp-111, Thr-113, Phe-115, Phe-122, and Leu-300, which lodges the nonpolar part of the inhibitor. Although the charge state of the cofactor (NADPH vs NADP<sup>+</sup>) has been shown not to be critical for inhibitor binding to ALR2,<sup>18</sup> it has been conclusively demonstrated that negatively charged ARIs act primarily by binding to the enzyme complexed with the oxidized NADP<sup>+</sup> to form a ternary dead-end complex that prevents turnover in the steady state.<sup>19</sup> Modeling studies, on the other hand, have suggested that a phenoxy group can provide a good structural replacement for the carboxylate group,<sup>20</sup> which can account for the ALR2 inhibitory activity of flavonoid compounds such as quercetin and the structure-based designed 7-hydroxy-2-(4'-hydroxybenzyl)-4*H*-1-benzopyran-4-one.<sup>21</sup>

Even though numerous clinical trials for the treatment of diabetic neuropathy have been conducted over the last 18 years with synthetic ARIs, pharmacokinetic



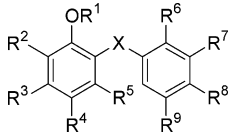
**Figure 3.** Some marine natural polybrominated diphenyl ethers.

problems, together with the length of the trials, have resulted in a lack of observed efficacy.<sup>22</sup> Thus, there is still an urgent need for new ARIs. In the following, we report on the ALR2 inhibitory properties of a marine natural product and a series of related novel polyhalogenated diphenyl ether derivatives. Their structure–activity relationships (SAR) have been rationalized on the basis of molecular modeling studies encompassing automated docking, molecular dynamics simulations, and free energy perturbation calculations.

## Results and Discussion

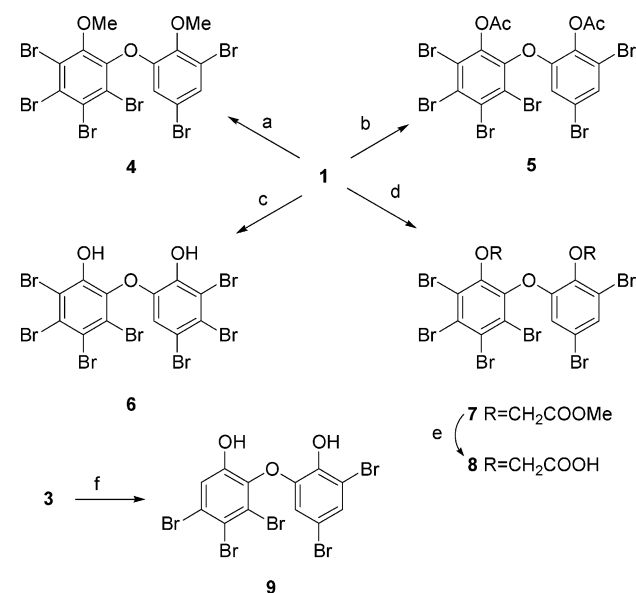
**Chemistry and Human ALR2 Inhibitory Activity.** In our search for new such ARIs, about 2000 marine natural products from our compound library were systematically screened. Potent inhibitory activity against human ALR2 (hALR2) was found in the polybrominated diphenyl ether **1** (Figure 3), a compound previously isolated from the marine sponge *Dysidea herbacea*.<sup>23</sup> It was noteworthy that this marine natural product showed an inhibitory activity (IC<sub>50</sub> = 6.4 μM) similar to that of the well-known ARI sorbinil (IC<sub>50</sub> = 3.6 μM) despite the absence of either a carboxylate or a cyclic imide group in its molecule. Two more natural polybrominated diphenyl ethers, **2** and **3** (Figure 3), isolated from the same sponge and closely related to **1**, were also assayed. Compound **3** showed no significant activity against hALR2 whereas **2** was shown to be only weakly active (Table 1). To the best of our knowledge, the only polybrominated diphenyl ether that has been previously reported as an ARI is 2',3,4,4',5-pentabromo-2-hydroxydiphenyl ether,<sup>24</sup> although some related polybrominated phenoxyphenols (including **1** and **3**) have been shown to be micromolar inhibitors of 15-lipoxygenase and inosine monophosphate dehydrogenase.<sup>25</sup> This fact highlights the need to address in more detail the issue of selectivity in future studies. For the time being, and in view of the encouraging preliminary findings, we have focused on the potential of these compounds as hALR2 inhibitors. A variety of new analogues were synthesized and tested (Table 1) to expand the SAR. Our results show the importance for this activity of both the hydroxyl groups and the bromine atom at the para position relative to the hydroxyl group.

Some of these analogues were obtained by modification of the marine natural products (Scheme 2). Thus, **6** was obtained by bromination of **1**. The chemical shift of the aromatic proton of **6** was at δ 6.69 indicating that this proton was ortho to the ether group, as pointed out previously.<sup>26</sup> The substitution pattern of all the other derivatives with halogen atoms at C-3, C-4, and C-5 was established by chemical shift comparison to the previous compounds.

**Table 1.** Human ALR2 Inhibitory Activities of the Test Compounds and Some Standard Inhibitors


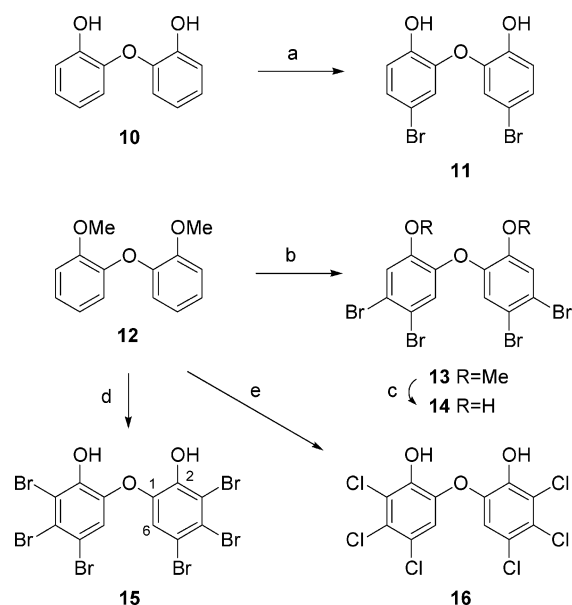
compd	X	R <sup>1</sup>	R <sup>2</sup>	R <sup>3</sup>	R <sup>4</sup>	R <sup>5</sup>	R <sup>6</sup>	R <sup>7</sup>	R <sup>8</sup>	R <sup>9</sup>	IC <sub>50</sub> (μM) <sup>a</sup>
<b>1</b>	O	H	Br	Br	Br	Br	OH	Br	H	Br	6.4 ± 1.1
<b>2</b>	O	H	Br	Br	H	Br	OH	Br	H	Br	25%
<b>3</b>	O	Me	H	Br	Br	Br	OMe	Br	H	Br	0%
<b>4</b>	O	Me	Br	Br	Br	Br	OMe	Br	H	Br	0%
<b>5</b>	O	Ac	Br	Br	Br	Br	OAc	Br	H	Br	0%
<b>6</b>	O	H	Br	Br	Br	Br	OH	Br	Br	Br	5.5 ± 1.4
<b>7</b>	O	CH <sub>2</sub> COOMe	Br	Br	Br	Br	OCH <sub>2</sub> COOMe	Br	H	Br	0%
<b>8</b>	O	CH <sub>2</sub> COOH	Br	Br	Br	Br	OCH <sub>2</sub> COOH	Br	H	Br	25 ± 0.1
<b>9</b>	O	H	H	Br	Br	Br	OH	Br	H	Br	0%
<b>11</b>	O	H	H	H	Br	H	OH	H	H	Br	32%
<b>13</b>	O	Me	H	Br	Br	H	OMe	H	Br	Br	0%
<b>14</b>	O	H	H	Br	Br	H	OH	H	Br	Br	46%
<b>15</b>	O	H	Br	Br	Br	H	OH	Br	Br	Br	5.7 ± 1.6
<b>16</b>	O	H	Cl	Cl	Cl	H	OH	Cl	Cl	Cl	3.2 ± 1.4
<b>20</b>	O	Me	Br	Br	Br	Br	OH	Br	H	OH	0%
<b>21</b>	O	H	Br	Br	Br	Br	OH	Br	H	OH	38%
<b>24</b>	O	H	Br	Br	Br	H	NH <sub>2</sub>	Br	Br	Br	8.9 ± 4.2
<b>27</b>	O	H	Br	Br	Br	H	OH	Br	OH	Br	4.4 ± 2.5
<b>30</b>	O	H	Br	Br	Br	Br	OH	Br	Br	F	3.2 ± 2.8
<b>32</b>	NH	Me	Br	Br	Br	H	OMe	Br	Br	Br	0%
<b>33</b>	NH	H	Br	Br	Br	H	OH	Br	Br	Br	18%
tolrestat											0.4 ± 0.3
sorbinil											3.6 ± 1.0
quercetin											14%

<sup>a</sup> IC<sub>50</sub> values represent the concentration required to produce 50% enzyme inhibition or percent of inhibition at the highest concentration used (25 μg/mL). Human recombinant ALR2 was used and all values are the mean of at least three experiments.

**Scheme 2<sup>a</sup>**

<sup>a</sup> Reagents and conditions: (a) K<sub>2</sub>CO<sub>3</sub>, MeI, 50 °C; (b) Ac<sub>2</sub>O, Pyr, rt; (c) Br<sub>2</sub>, AcOH, 90 °C; (d) K<sub>2</sub>CO<sub>3</sub>, acetone, BrCH<sub>2</sub>COOMe, 65 °C; (e) KOH, EtOH, 90 °C; (f) BBr<sub>3</sub>, ClCH<sub>2</sub>CH<sub>2</sub>Cl, rt.

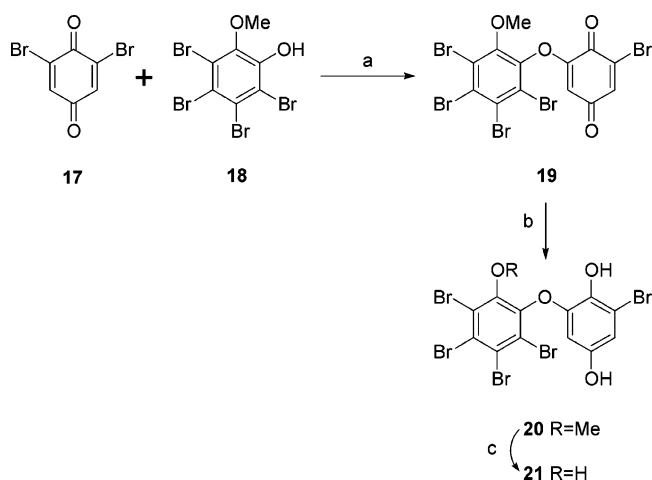
Novel polyhalogenated diphenyl ether derivatives were obtained by total synthesis (Schemes 3 and 4). Treatment of the known **12** with bromine afforded **13**, which was transformed into **14** by treatment with boron tribromide. NOESY experiments of **13** showed correlations between the methoxy group and the proton at δ 7.19, indicating that the bromine atoms were meta and para to the phenolic OH. This assignment was also confirmed by Heteronuclear Multiple Bond Coherence

**Scheme 3<sup>a</sup>**

<sup>a</sup> Reagents and conditions: (a) Br<sub>2</sub>, CHCl<sub>3</sub>, -35 °C; (b) Br<sub>2</sub>, AcOH, rt; (c) BBr<sub>3</sub>, ClCH<sub>2</sub>CH<sub>2</sub>Cl, rt; (d) Br<sub>2</sub>, AcOH, reflux; (e) AlCl<sub>3</sub>, SO<sub>2</sub>Cl<sub>2</sub>, 95 °C.

experiments of **14**. Other analogues were obtained by use of the Ullmann reaction between guaiacol and different bromobenzenes in the presence of copper catalyst<sup>27</sup> (Scheme 5). Compound **31** (Scheme 6) was obtained as previously described<sup>28</sup> and was used to obtain the derivatives **32** and **33**.

The effect of hydroxyl group modification can be assessed by comparing compound **1** with compounds **4**, **5**, and **7**; the resulting complete loss of activity strongly

Scheme 4<sup>a</sup>

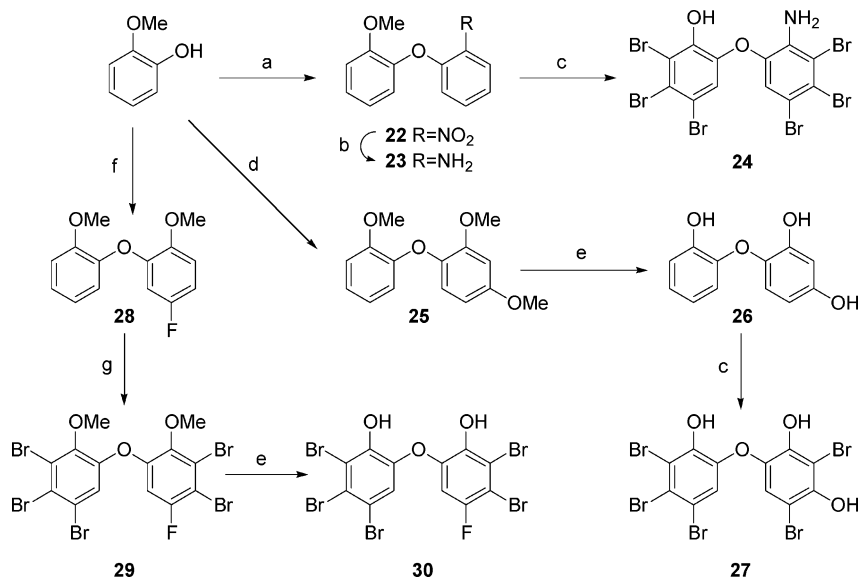
<sup>a</sup> Reagents and conditions: (a)  $K_2CO_3$ , DMF, rt; (b)  $Na_2S_2O_4$ ,  $CHCl_3/H_2O$ , rt; (c)  $BBR_3$ ,  $ClCH_2CH_2Cl$ , rt.

suggests that these free hydroxyl groups play a significant role in enzyme binding. This could be due to steric hindrance or to a direct involvement of one or both OH groups in crucial interactions with the enzyme binding site; an alternative possibility would be that a conformational change takes place on the inhibitor upon substitution that is incompatible with binding at the site. Further data confirm this SAR, as compounds **13**, **20**, and **32**, all of them with methoxy groups in place of the hydroxyls, showed no activity, whereas the corresponding compounds with free hydroxyl groups **14**, **21**,

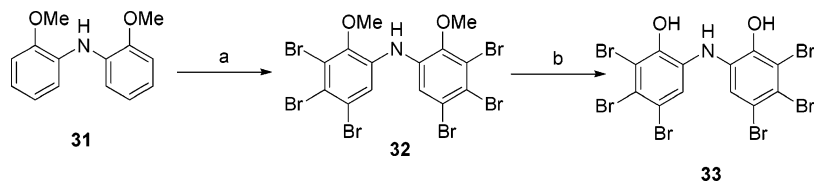
and **33**, respectively, were modestly active. On the other hand, incorporation of two methylenecarboxylic groups in place of the hydroxyls, as in **8**, led to an active product even though its inhibitory properties were decreased with respect to the parent compound. For other phenolic ARIs related to acetophenones and benzophenones,<sup>29</sup> as well as several hydroxylated chalcones and benzopirane-4-ones,<sup>21</sup> the markedly detrimental effect on biological activity of methylation of the hydroxyl groups has been taken as evidence for the involvement of the dissociated phenoxy forms in binding to the enzyme. However, in the present series, substitution of an amino group for one of the hydroxyls (as in going from **15** to **24**) had just a marginal deleterious effect on the inhibitory activity, suggesting that this particular hydroxyl group participates in donating a hydrogen bond to the enzyme binding site. On the other hand, comparison of the activities of compounds **15** and **33** clearly illustrates that an amino group can replace the bridging ether group but only at a great cost in potency.

To assess the importance of the halogen group in the meta position relative to the bridging ether oxygen we pairwise compared the activities of compounds **1** and **9**, **1** and **21**, and **14** and **15**. From these results (Table 1) it can be inferred that replacement of a bromine at this meta position with either a hydrogen or a hydroxyl group is detrimental for potency, regardless of the ring in which this substitution takes place.

The importance of the halogen group at the para position with respect to the ether oxygen in any of the rings was evaluated by comparing the pairs **1** and **6**,

Scheme 5<sup>a</sup>

<sup>a</sup> Reagents and conditions: (a) NaH,  $CuBr \cdot SMe_2$ , DMF, 1-bromo-2-nitrobenzene, reflux; (b) 10% Pd/C,  $H_2$ , MeOH; (c)  $Br_2$ ,  $CCl_4$ , rt; (d) NaOMe, CuCl, Pyr, 1-bromo-2,5-dimethoxybenzene, reflux; (e)  $BBR_3$ ,  $ClCH_2CH_2Cl$ , rt; (f) NaOMe, CuCl, Pyr, 2-bromo-4-fluoroanisole, reflux; (g)  $Br_2$ , AcOH, rt.

Scheme 6<sup>a</sup>

<sup>a</sup> Reagents and conditions: (a)  $Br_2$ ,  $CCl_4$ , rt; (b)  $BBR_3$ ,  $ClCH_2CH_2Cl$ , rt.

**Table 2.** Inhibitory Activity on Sorbitol Accumulation in Human Retinal Cells

compd	IC <sub>50</sub> (μM) <sup>a</sup>
<b>1</b>	3
<b>6</b>	7
<b>15</b>	1
<b>16</b>	0.24
<b>24</b>	6
<b>27</b>	8
<b>30</b>	11
tolrestat	0.02
sorbinil	4

<sup>a</sup> IC<sub>50</sub> values represent compound concentration that inhibited sorbitol accumulation by 50%. Retinal human cells were used and all values are the mean of at least three experiments.

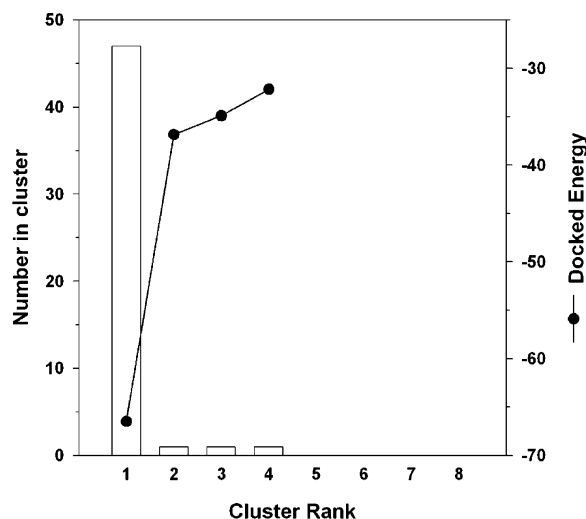
and **15** and **27**. Given their similar activities, our conclusion is that the nature of the substituent at this para position (a bromine, a hydroxyl or a hydrogen) is not crucial for modulating the inhibitory properties of these compounds. The same reasoning can be applied to the ortho position relative to the bridging ether oxygen since replacement of a bromine, as in **1** and **6**, with a hydrogen (compound **15**) had no effect on potency.

Compounds **16** and **30**, in which one or some of the bromine atoms of **1** or **15** have been replaced with chlorine or fluorine, allowed us to assess the relative importance of different halogen atoms on activity. The potency in both cases increased only 2-fold, which suggests that the type of halogen has little bearing on the inhibitory activity.

Those compounds with an in vitro IC<sub>50</sub> ≤ 10 μM were then advanced to a secondary screen in which compounds were tested for their ability to prevent the accumulation of sorbitol inside human retinal cells when they were cultured in a medium supplemented with 50 mM glucose so as to reproduce in vitro the typical hyperglycemic conditions of diabetes. The results show that six out of the seven compounds tested in this assay have an IC<sub>50</sub> under 10 μM (Table 2). Interestingly, the potency of compounds **15** and **16** was 4-fold and 17-fold greater, respectively, than that of sorbinil. Moreover, in this assay compound **16** was 12 times more potent, on a molar basis, than the lead marine natural product **1**.

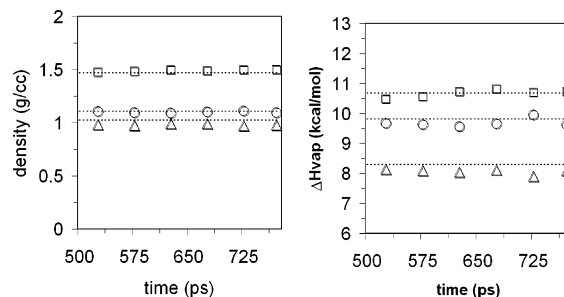
**Molecular Modeling of hALR2 and Docking of the Inhibitors.** A structure for the hALR2:NADP<sup>+</sup>:zopolrestat ternary complex was modeled starting from the coordinates deposited for the Cα trace of the enzyme, the cofactor NADP<sup>+</sup>, and the inhibitor (PDB accession code: 1mar),<sup>15</sup> as described in the Experimental Section. Energy refinement of this complex resulted in an enzyme structure possessing an enlarged active site in an "open" conformation that was suitable for inhibitor binding. Prior to automated docking of the reported novel inhibitors, zopolrestat itself was docked as a means of testing program performance. The largest cluster found also corresponded to the lowest docking energy and contained the crystallographic solution (Figure 4).

Since the reported inhibitors are halogenated and no parameters were available for these atoms in the molecular mechanics force field AMBER (parm96),<sup>30</sup> consistent parameters for the halogen atoms had to be derived to describe the bonded and nonbonded interactions (Table 3). Calibration of these crucial parameters

**Figure 4.** AutoDock results for docking zopolrestat into the modeled hALR2 enzyme.**Table 3.** Bonded and Nonbonded Parameters for the Halogen Atoms Present in the Halobenzenes Studied

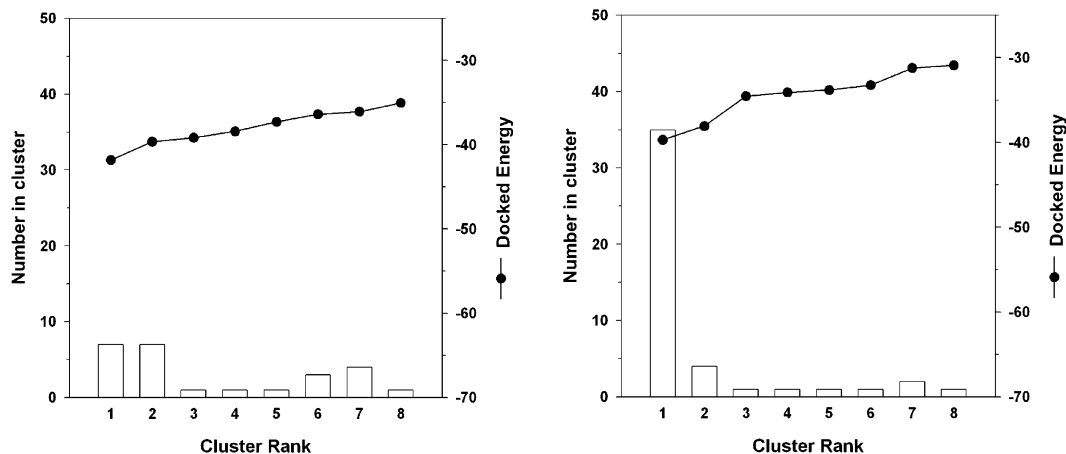
bond	K <sub>r</sub> <sup>a</sup>	r <sub>eq</sub> <sup>b</sup>	angle	K <sub>θ</sub> <sup>c</sup>	θ <sub>eq</sub> <sup>d</sup>	atom	R <sup>*a</sup>	ε <sup>b</sup>
CA-F	386.0	1.331	CA-CA-F	70.0	119.0	F	1.63	0.171
CA-Cl	193.0	1.745	CA-CA-Cl	70.0	119.0	Cl	1.82	0.475
CA-Br	172.0	1.888	CA-CA-Br	70.0	119.0	Br	1.94	0.595

<sup>a</sup> Bond force constant, kcal/(mol Å<sup>2</sup>). <sup>b</sup> Equilibrium bond lengths, Å. <sup>c</sup> Angle bending force constant, kcal/(mol radian<sup>2</sup>). <sup>d</sup> Equilibrium bond angles (deg). <sup>e</sup> van der Waals minimum. <sup>f</sup> van der Waals well depth.

**Figure 5.** Time evolution of (left) the calculated density (g cm<sup>-3</sup>) and (right) enthalpy of vaporization (ΔH<sub>vap</sub>, kcal/mol) during the molecular dynamics simulations of the solvent dynamics: fluorobenzene (open triangles), chlorobenzene (open circles), and bromobenzene (open squares). For comparative purposes, dotted lines have been drawn at the respective experimental values.

was achieved using condensed phase molecular dynamics simulations of three relevant organic solvents (see under Computational Methods). The good agreement found between the calculated and experimentally measured densities and enthalpies of vaporization of these liquids (Figure 5) attests to the validity of these parameters, which were similar but not equivalent to previously reported parameters for the same atoms in haloalkanes.<sup>31</sup>

The nonbonded parameters were also transformed into a form suitable for the automated docking program (see Methodology and Supporting Information). The docking results for the diphenyl ethers inhibitors were heavily dependent on the degree of halogenation. Thus, for compound **1** a large number of solutions, all of them outside the active site, were found whereas compound **16** was preferably docked within the specificity pocket



**Figure 6.** AutoDock results for representative compounds **1** (left) and **16** (right) into the modeled hALR2 enzyme.

of the active site (Figure 6). The calculated binding energies, however, were very similar in both cases and, rather strikingly, could not be used to tell apart those molecules that were bound in the active site from those bound elsewhere. The preferred orientation found for **16** was chosen as the most plausible one also for **1** and the remaining inhibitors. The differences observed between **1** and **16** were thought to arise from the increased size of bromine relative to chlorine, which can hamper docking into the rigidly fixed binding site.

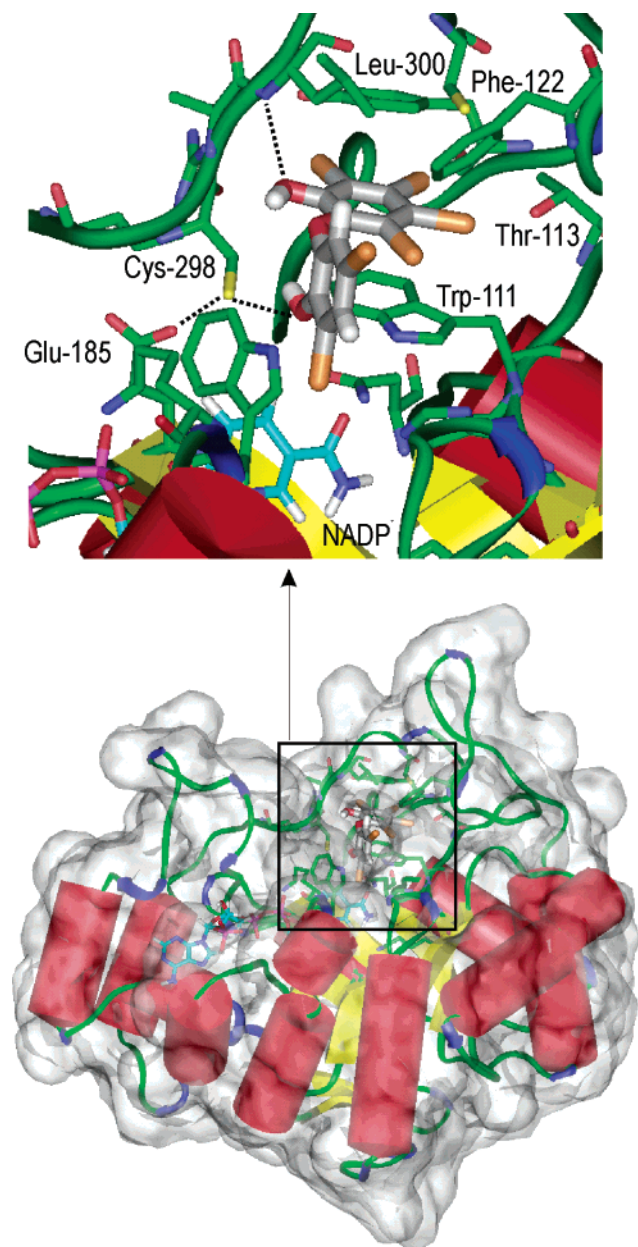
To assess the feasibility of the proposed binding orientation and study the mutual adaptation between enzyme and inhibitor, the hALR2–NADP<sup>+</sup>–**1** ternary complex was energy-minimized and simulated for 950 ps of molecular dynamics. The average structure was then analyzed in terms of intermolecular energy components, desolvation effects, and conformational changes with respect to the holoenzyme (apoenzyme + coenzyme).

In the native human holoenzyme (PDB code: 1ads)<sup>14</sup> the side chain of Leu300 makes a direct contact with the aromatic ring of Trp111. The binding orientation we propose for **1** is such that the more heavily halogenated phenyl ring is sandwiched between the indole ring of Trp-111 on one side and the side chains of Leu-300 and Cys-303 on the other side (Figure 7). This hydrophobic interaction, which is similar but not identical to that described for the larger benzothiazole ring of zopolrestat,<sup>15</sup> is further stabilized by the phenyl ring of Phe-122, whose edge contacts both halogenated phenyl rings. The ether oxygen allows a nearly orthogonal orientation of these two rings with respect to each other such that the electronegative bromine atom ortho to the hydroxyl group in the second phenyl ring makes contact with both Trp-20 and the pyridinium group of NADP<sup>+</sup>. The free hydroxyls engage in hydrogen bonding interactions with the NH of Leu-300 (the OH acts as an acceptor) and the thiol group of Cys-298 (the OH acts as a donor). The position of this latter sulfhydryl group is fixed by a buttressing interaction from the carboxylate of Glu-185. The inhibitor is thus almost completely sequestered from the solvent in the apolar region of the pocket whereas it occupies the polar region of the binding site only partially. Overall, the orientation is reminiscent of that of bound zopolrestat and differs with respect to that of tolrestat (Figure 2). However, the structural similarity is much greater with the recently

reported complex of hALR2 with zenarestat,<sup>32</sup> an inhibitor that also contains a bihalogenated phenyl ring (Figures 1 and 2).

The proposed binding mode can rationalize the SAR reported above. Replacement of the ether bridge with an amino group, as in going from **15** to **33**, will bring about a detrimental change in the intra- and intermolecular hydrogen bonding patterns resulting in much lower affinity (Table 1). Incorporation of two methyl-encarboxylic groups in place of the hydroxyls, as in going from **1** to **8**, will likewise result in loss of potency due to the increase in bulk in positions that are in very close contact with protein atoms and engaged in crucial hydrogen bonding interactions. The irrelevant nature of the substituents present at the ortho and para positions relative to the bridging ether oxygen is now rationalized because these positions are mostly exposed to the bulk solvent.

**Energy Analysis of the Enzyme–Inhibitor Complexes.** The energy analysis of the hALR2–NADP<sup>+</sup>–**1** complex (Figure 8) reveals a predominance of van der Waals interactions involving (in decreasing order of magnitude) Trp-111, Leu-300, Trp-20, Cys-298, Cys-303, NADP<sup>+</sup>, Phe-122, Tyr-309, His-110, and Ala-299. The electrostatic interactions, on the other hand, appear to be dominated by Cys-298, followed by Lys-77, Trp-111, Leu-300, and NADP<sup>+</sup>. When compared with zopolrestat (Figure 1 of the Supporting Information), the major differences in electrostatic interaction energy between these two compounds and the enzyme originate from those residues that interact with the free carboxylate group of this negatively charged inhibitor, that is, Lys-77 and NADP<sup>+</sup>. However, the counterparts of these favorable intermolecular interactions are a larger repulsion with negatively charged residues, such as Asp-43 and Glu-185, and a larger desolvation penalty associated with the removal of the interacting polar groups from water. Thus, in the hALR2:NADP<sup>+</sup>:**1** complex, the electrostatic contributions to the free energy change associated with desolvation of both the binding site and the inhibitor are 4.6 and 1.9 kcal mol<sup>-1</sup>, respectively, whereas for the hALR2:NADP<sup>+</sup>:zopolrestat complex the corresponding values are 7.2 and 13.3 kcal mol<sup>-1</sup>. Since the sum of all residue-based electrostatic contributions to the binding energy is –14.1 kcal mol<sup>-1</sup> for zopolrestat versus –2.2 kcal mol<sup>-1</sup> for **1**, the net electrostatic



**Figure 7.** Proposed binding site for **1** in hALR2. (bottom) Schematic representation of the  $C\alpha$  trace of the enzyme ( $\alpha$ -helices are shown as red barrels,  $\beta$ -strands as yellow flat ribbons, and turns as blue arrows), with protein residues enveloped by a semitransparent solvent-accessible surface. Carbon atoms of  $NADP^+$  and the inhibitor are colored in cyan and gray, respectively. (top) Enlarged view of the framed area shown in the top panel. Protein residues relevant to the discussion have been labeled, and their side chains are shown as sticks.

binding free energy difference between the two compounds is only 2 kcal mol<sup>-1</sup>.

Finally, a thermodynamic cycle (Scheme 7) was set up to test whether the proposed binding orientation could account for the importance of the crucial bromine atom in the para position that distinguishes the active **1** from the much less active **2**.

Although an increase in hydrophobicity is expected in going from H to Cl or Br, as assessed from the incremental  $\pi$  constants derived from log  $P_{o/w}$  values for benzene derivatives,<sup>33</sup> such a change is not always directly correlated with an increase in activity although

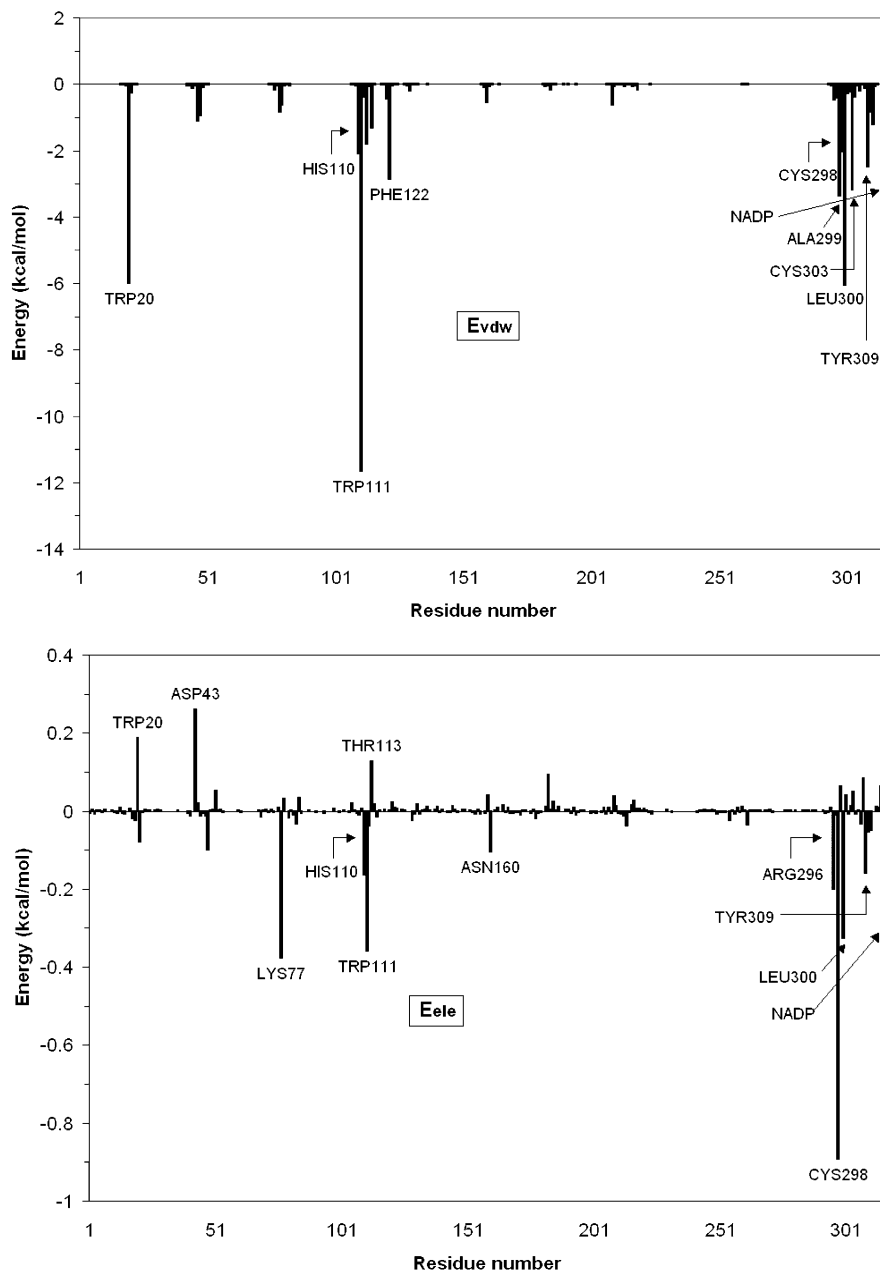
it usually is in very good agreement with calculated differences in solvation free energies, as we have recently shown for an unrelated series of antiviral compounds.<sup>34</sup>

The free energy difference associated with conversion of **1** into **2** in aqueous solution was  $-5.83 \pm 0.04$  kcal mol<sup>-1</sup>, in very good agreement with the change of  $5.90 \pm 0.04$  kcal mol<sup>-1</sup> obtained from the independent perturbation of **2** into **1**. For the perturbations of the enzyme-bound inhibitors the corresponding free energy changes were  $-4.33 \pm 0.52$  kcal mol<sup>-1</sup> and  $3.60 \pm 0.52$  kcal mol<sup>-1</sup>, respectively. The binding of **2** to hALR2 is thus calculated to be disfavored by  $1.50 \pm 0.30$  kcal mol<sup>-1</sup> with respect to the binding of **1**, which is in semiquantitative agreement with the decreased potency shown by **2** in the enzyme inhibition assay relative to **1** (Table 1). It is remarkable that this relatively large difference stems from a simple Br  $\rightarrow$  H substitution in an otherwise equally polyhalogenated compound, but the more favorable binding energy can be related to both improved interactions with the enzyme and to a greater hydrophobic effect. This bromine atom is lodged in a pocket (made up by Trp-79, Trp-111, Thr-113, Phe-115, and Cys-303) that is enlarged upon minor side-chain conformational changes. Interestingly, the position of this deeply buried bromine atom is spatially equivalent to that occupied by the only bromine atom present in zenarestat (Figure 1). The fact that introduction of this halogen atom alone into a weak inhibitor is enough to turn it into a more potent one can be important for future ARI design using a minimal molecular framework.

## Conclusions

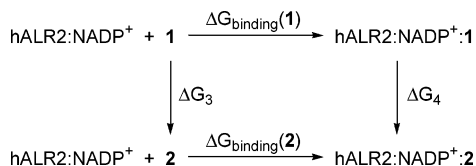
A marine natural polybrominated diphenyl ether, **1**, has been identified as a new hALR2 inhibitor having an IC<sub>50</sub> of 6.4  $\mu$ M, and a series of analogues have been synthesized and evaluated to establish the structure–activity relationships. The most notable structural feature of the active compounds is the lack of either the carboxylate or the cyclic imide group commonly present in the principal classes of currently used inhibitors. Several of the synthetic derivatives were marginally more active than the lead compound in the in vitro assay and one of them, **16**, was able to prevent sorbitol accumulation inside human retinal cells at concentrations 17-fold lower than were necessary with the standard drug sorbinil.

The crucial role of one of the bromine atoms in **1** was realized when a molecular model of the complex was constructed and simulated using molecular dynamics. The spatial position of the relevant Br atom in the specificity pocket of the active site is coincident with that of the bromine atom present in zenarestat. Moreover, the described inhibitors and zenarestat give rise to similar conformational changes in the enzyme. Further support for the proposed binding mode was inferred from the good qualitative agreement that was obtained between the experimentally measured differences in inhibitory activity and the calculated differences in binding free energies using a free energy perturbation approach.



**Figure 8.** Calculated van der Waals (top) and continuum electrostatic (bottom) interaction energies between **1** and individual protein and cofactor residues.

#### Scheme 7<sup>a</sup>



<sup>a</sup> Thermodynamic cycle used to estimate the free energy changes involved when a bromine in **1** is replaced with a hydrogen (as in **2**) in the free ligand in solution ( $\Delta G_3$ ) and in the solvated complex ( $\Delta G_4$ ), respectively.

#### Experimental Section

**A. Chemical Procedures.** Melting points were determined in open capillaries with a Büchi B-535 melting point apparatus and are uncorrected. The NMR spectra were recorded on a Varian 300 spectrometer at 300 MHz for <sup>1</sup>H NMR and at 75 MHz for <sup>13</sup>C NMR, with TMS as an internal standard. Chemical shifts ( $\delta$ ) are reported as s (singlet), d (doublet), t (triplet), q (quartet), m (multiplet), or br s (broad singlet).

Elemental analyses were performed on a Perkin-Elmer analyzer (model 2400 CHN). ESI and APCI mass spectra were recorded on a HP 1100 LC/MS, EI and FAB mass spectra on a VG Autospec spectrometer. Thin-layer chromatography was performed on Merck silica gel plates (DC-60 F<sub>254</sub>). SDS silica gel (35–70  $\mu\text{m}$ ) and Merck RP-18 (40–63  $\mu\text{m}$ ) were used for normal and reverse phase flash chromatography, respectively. All reagents were used as received unless otherwise stated.

Compounds **1–3** were isolated from the sponge *Dysidea herbacea* as previously described,<sup>23</sup> and were identical in all respects to those reported in the literature. Compounds **4**,<sup>26</sup> **10**,<sup>35</sup> and **11**<sup>36</sup> were obtained as previously described.

**3,3',4,5,5',6-Hexabromo-2,2'-diacetoxydiphenyl Ether (5).** To a solution of **1** (5 mg, 8  $\mu\text{mol}$ ) in pyridine (0.4 mL) was added Ac<sub>2</sub>O (0.4 mL). The mixture was stirred at room temperature for 24 h and concentrated in vacuo. The residue was chromatographed on a silica gel column (Hex–CH<sub>2</sub>Cl<sub>2</sub>, 1:1) to afford **5** (5.4 mg, 96%): <sup>1</sup>H NMR (CDCl<sub>3</sub>):  $\delta$  7.48 (s, 1H), 7.47 (s, 1H), 2.35 (s, 3H), 2.24 (s, 3H). MS (ESI-negative) *m/z*: 717 [M – Ac]<sup>–</sup>, 674 [M – 2Ac]<sup>–</sup>.

**3,3',4,4',5,5',6-Heptabromo-2,2'-dihydroxydiphenyl Ether (6).** To a solution of **1** (50 mg, 74  $\mu$ mol) in acetic acid (5 mL) at room temperature and stirring was added bromine (0.5 mL, 9.76 mmol). The mixture was heated for 3 days at 90–95 °C and then cooled to room temperature and concentrated in vacuo. The residue was chromatographed on a silica gel column (Hex–acetone, 3:2) to afford **6** (32 mg, 57%): mp: 188–190 °C; <sup>1</sup>H NMR (CD<sub>3</sub>OD):  $\delta$  6.69 (s, 1H); <sup>13</sup>C NMR (CD<sub>3</sub>OD):  $\delta$  150.49, 146.81, 145.54, 141.11, 126.94, 121.97, 121.30, 118.92, 117.92, 116.40, 115.58, 113.75; MS (APCI-negative) *m/z*: 753 [M – H]<sup>–</sup>, 674 [M – Br]<sup>–</sup>. Anal. (C<sub>12</sub>H<sub>3</sub>Br<sub>7</sub>O<sub>3</sub>) C; H: calcd, 0.40; found, 0.36.

**3,3',4,5,5',6-Hexabromo-2,2'-dimethoxycarbonylmethoxydiphenyl Ether (7).** To a solution of **1** (9 mg, 13  $\mu$ mol) and BrCH<sub>2</sub>COOMe (0.4 mL, 4.2 mmol) in acetone (2 mL) was added K<sub>2</sub>CO<sub>3</sub> (5 mg, 35  $\mu$ mol). After stirring at 65 °C for 6 h, the reaction was cooled to room temperature and filtered. The solvent was removed in vacuo, and the residue was chromatographed on a silica gel column (Hex–EtOAc, 8:2) to afford **7** (9.9 mg, 91%): <sup>1</sup>H NMR (CDCl<sub>3</sub>):  $\delta$  7.43 (d, *J* = 2.2 Hz, 1H), 6.49 (d, *J* = 2.2 Hz, 1H), 4.75 (s, 2H), 4.67 (s, 2H), 3.80 (s, 3H), 3.75 (s, 3H); <sup>13</sup>C NMR (CDCl<sub>3</sub>):  $\delta$  168.51, 167.68, 149.77, 148.91, 144.10, 143.78, 130.08, 126.98, 125.12, 122.31, 121.36, 118.92, 117.52, 117.06, 69.73, 69.58, 52.39, 52.21. MS (ESI-positive) *m/z*: 843 [M + Na]<sup>+</sup>. Anal. (C<sub>18</sub>H<sub>12</sub>Br<sub>6</sub>O<sub>7</sub>) C; H: calcd, 1.48; found, 1.45.

**3,3',4,5,5',6-Hexabromo-2,2'-dicarboxymethoxydiphenyl Ether (8).** A mixture of **7** (10 mg, 12  $\mu$ mol), 10% KOH (0.05 mL, 0.89 mmol) and ethanol (3 mL) was heated at 90 °C for 2 h. The reaction mixture was cooled to room temperature and concentrated in vacuo. The residue was poured into H<sub>2</sub>O, acidified with 1M HCl to pH = 5 and extracted with EtOAc. The organic layers was washed with H<sub>2</sub>O and brine, dried (Na<sub>2</sub>SO<sub>4</sub>) and removed in vacuo to give **8** (9.6 mg, 96%): mp: 185–187 °C; <sup>1</sup>H NMR (DMSO-*d*<sub>6</sub>):  $\delta$  7.58 (d, *J* = 2.4 Hz, 1H), 6.96 (d, *J* = 2.4 Hz, 1H), 4.65 (s, 2H), 4.51 (s, 2H); <sup>13</sup>C NMR (DMSO-*d*<sub>6</sub>):  $\delta$  169.43, 168.75, 149.86, 149.26, 143.72, 143.53, 129.10, 126.22, 123.96, 122.04, 121.01, 118.18, 117.09, 116.29, 69.91, 69.56; MS (FAB-positive) *m/z*: 814 [M + Na]<sup>+</sup>. Anal. (C<sub>16</sub>H<sub>8</sub>Br<sub>6</sub>O<sub>7</sub>) C; H: calcd, 1.02; found, 1.10.

**3,4',5,5',6'-Pentabromo-2,2'-dihydroxydiphenyl Ether (9).** To a solution of **3** (2 mg, 3.2  $\mu$ mol) in 1,2-dichloroethane (2 mL) was added dropwise boron tribromide<sup>37</sup> (100  $\mu$ L, 1 mmol) under an argon atmosphere. The mixture was stirred at room temperature overnight. Diethyl ether was added dropwise, and after stirring for 15 min, the mixture was diluted with EtOAc, washed with H<sub>2</sub>O, dried (Na<sub>2</sub>SO<sub>4</sub>), and concentrated in vacuo. The residue was chromatographed on a silica gel column (Hex–EtOAc, 8:2) to afford the known **9** (1.5 mg, 79%), which was identified by comparison of the <sup>1</sup>H NMR and MS data with published values.<sup>25</sup>

**4,4',5,5'-Tetrabromo-2,2'-dimethoxydiphenyl Ether (13).** To solution of **12**<sup>35</sup> (200 mg, 0.87 mmol) in acetic acid (5 mL) was added dropwise bromine (1 mL) while stirring. The mixture was stirred at room temperature for 1 h and then was concentrated in vacuo. The residue was treated with 1M NaOH and extracted with CH<sub>2</sub>Cl<sub>2</sub>. The combined organic layers were washed successively with H<sub>2</sub>O and brine, dried (Na<sub>2</sub>SO<sub>4</sub>), and concentrated in vacuo to give quantitatively **13** (474 mg): mp 134–135 °C; <sup>1</sup>H NMR (CDCl<sub>3</sub>):  $\delta$  7.19 (s, 2H), 7.02 (s, 2H), 3.83 (s, 6H); a correlation was observed in a NOESY spectrum in this solvent between  $\delta$  3.83 and 7.19; <sup>13</sup>C NMR (CDCl<sub>3</sub>):  $\delta$  149.99, 144.72, 122.99, 119.13, 117.30, 114.75, 56.37. Anal. (C<sub>14</sub>H<sub>10</sub>Br<sub>4</sub>O<sub>3</sub>) C; H: calcd, 1.85; found, 1.86.

**4,4',5,5'-Tetrabromo-2,2'-dihydroxydiphenyl Ether (14).** Compound **14** was prepared from **13** (54 mg, 0.1 mmol) according to the method of preparation for **9**. The residue was chromatographed on a silica gel column (Hex–EtOAc, 3:2) to give **14** (49 mg, 95%): mp 195–197 °C. <sup>1</sup>H NMR (CD<sub>3</sub>OD):  $\delta$  7.23 (s, 2H), 7.06 (s, 2H); <sup>13</sup>C NMR (CD<sub>3</sub>OD):  $\delta$  149.65, 145.48, 124.28, 122.41, 119.78, 113.76; gHMBC correlations were observed between  $\delta$ 113.76 (C-4), 119.78 (C-5), 145.48 (C-2),

149.65 (C-1) and 7.23 (H-3) and 7.06 (H-6); MS (APCI-negative) *m/z*: 517 [M – H]<sup>–</sup>. Anal. (C<sub>12</sub>H<sub>6</sub>Br<sub>4</sub>O<sub>3</sub>) C; H: calcd, 1.17; found, 1.13.

**3,3',4,4',5,5'-Hexabromo-2,2'-dihydroxydiphenyl Ether (15).** To a solution of **12**<sup>35</sup> (200 mg, 0.99 mmol) in acetic acid (6 mL) at room temperature was added dropwise bromine (2 mL, 39.6 mmol) while stirring. The reaction mixture was heated for 15 h at 90–95 °C and then cooled to room temperature and concentrated in vacuo. The residue was chromatographed on a silica gel column (Hex–EtOAc, 7:3) to afford **15** (520 mg, 78%): mp 188–190 °C. <sup>1</sup>H NMR (CD<sub>3</sub>OD):  $\delta$  7.16 (s, 2H); <sup>13</sup>C NMR (CD<sub>3</sub>OD):  $\delta$  148.21, 145.29, 123.78, 122.98, 116.45, 114.43; MS (APCI-negative) *m/z*: 675 [M – H]<sup>–</sup>. Anal. (C<sub>12</sub>H<sub>4</sub>Br<sub>6</sub>O<sub>3</sub>) C; H: calcd, 0.90; found, 0.96.

**3,3',4,4',5,5'-Hexachloro-2,2'-dihydroxydiphenyl Ether (16).** A suspension of **12**<sup>35</sup> (120 mg, 0.5 mmol), aluminum trichloride (35 mg, 0.26 mmol) in sulfuryl chloride (2 mL) was heated at 95 °C for 6 h. The mixture was cooled to room temperature and concentrated in vacuo. The residue was taken up in EtOAc, washed with H<sub>2</sub>O and brine, dried (Na<sub>2</sub>SO<sub>4</sub>), and concentrated in vacuo. The residue was dissolved in 1,2-dichloroethane (4 mL) and boron tribromide (1.06 g, 4.23 mmol) was added dropwise under an argon atmosphere. The mixture was stirred at room temperature for 1 h. Diethyl ether was added dropwise, and after stirring for 15 min, the mixture was diluted with EtOAc, washed with H<sub>2</sub>O and brine, dried (Na<sub>2</sub>SO<sub>4</sub>), and concentrated in vacuo. The residue was chromatographed on a silica gel (RP-18) column (MeOH–H<sub>2</sub>O, 85:15) to give **16** (14 mg, 6%): <sup>1</sup>H NMR (acetone-*d*<sub>6</sub>):  $\delta$  7.28 (s, 2H); <sup>13</sup>C NMR (acetone-*d*<sub>6</sub>):  $\delta$  146.79, 144.43, 127.52, 123.08, 122.81, 119.26; MS (APCI-negative) *m/z*: 407 [M – 2H]<sup>–</sup>. Anal. (C<sub>12</sub>H<sub>4</sub>Cl<sub>6</sub>O<sub>3</sub>) C; H: calcd, 0.99; found, 1.03.

**2-Bromo-6-(2,3,4,5-tetrabromo-6-methoxy-phenoxy)-1,4-benzoquinone (19).** A displacement reaction<sup>38</sup> of one bromine atom from 2,6-dibromobenzoquinone was used to obtain **19**. To this end, to a solution of **18**<sup>39</sup> (300 mg, 0.68 mmol) in DMF (9 mL) was added K<sub>2</sub>CO<sub>3</sub> (189 mg, 1.36 mmol). The mixture was stirred at room temperature for 1 h before adding a solution of **17**<sup>40</sup> (181 mg, 0.68 mmol) in DMF (6 mL). After 2 and 5 h at room-temperature two more additions of **17** (203 mg, 0.76 mmol) were done. The mixture was stirred at room temperature for 24 h, and then it was treated with HCl (2 M), extracted with diethyl ether, washed with brine, dried (Na<sub>2</sub>SO<sub>4</sub>), and concentrated in vacuo. The residue was chromatographed on a silica gel column (Hex–CH<sub>2</sub>Cl<sub>2</sub>, 3:2) to afford **19** (60 mg, 14%): <sup>1</sup>H NMR (CDCl<sub>3</sub>):  $\delta$  7.23 (d, *J* = 1.8 Hz, 1H), 5.67 (d, *J* = 1.8 Hz, 1H), 3.83 (s, 3H); <sup>13</sup>C NMR (acetone-*d*<sub>6</sub>):  $\delta$  183.98, 173.33, 154.47, 149.65, 143.95, 138.31, 134.56, 127.52, 124.88, 122.45, 119.89, 111.70, 61.90.

**3,3',4,5,6-Pentabromo-2-methoxy-2',5'-dihydroxydiphenyl Ether (20).** To a mixture of **19** (42 mg, 0.07 mmol) in CHCl<sub>3</sub> (2 mL) was added a solution of Na<sub>2</sub>S<sub>2</sub>O<sub>4</sub> (60 mg, 0.34 mmol) in H<sub>2</sub>O (2 mL). After being stirred for 5 h at room temperature, the reaction mixture was washed with brine, dried (Na<sub>2</sub>SO<sub>4</sub>), and concentrated in vacuo. The residue was chromatographed on a silica gel column (Hex–EtOAc, 9:1) to give **20** (26 mg, 62%): <sup>1</sup>H NMR (acetone-*d*<sub>6</sub>):  $\delta$  8.31 (s, 1H), 8.17 (s, 1H), 6.75 (d, *J* = 2.7 Hz, 1H), 6.05 (d, *J* = 2.7 Hz, 1H), 3.87 (s, 3H); <sup>13</sup>C NMR (acetone-*d*<sub>6</sub>):  $\delta$  152.30, 151.30, 146.78, 146.38, 137.82, 126.11, 124.45, 122.76, 122.42, 113.95, 111.22, 102.43, 61.99.

**3,3',4,5,6-Pentabromo-2,2',5'-trihydroxydiphenyl Ether (21).** To a solution of **20** (66 mg, 0.1 mmol) in 1,2-dichloroethane (4 mL) was added dropwise boron tribromide (0.03 mL, 0.3 mmol) under an argon atmosphere. The mixture was stirred at room temperature for 14 h. Diethyl ether was added dropwise, and after stirring for 15 min, the mixture was diluted with EtOAc, washed with H<sub>2</sub>O and brine, dried (Na<sub>2</sub>SO<sub>4</sub>), and concentrated in vacuo to afford **21** (50 mg, 80%): mp 216–218 °C. <sup>1</sup>H NMR (acetone-*d*<sub>6</sub>):  $\delta$  6.72 (d, *J* = 2.7 Hz, 1H), 6.01 (d, *J* = 2.7 Hz, 1H); <sup>13</sup>C NMR (acetone-*d*<sub>6</sub>):  $\delta$  151.37, 150.06, 145.91, 140.37, 137.91, 126.24, 121.31, 118.51, 115.41, 113.75, 111.1, 101.68; MS (ESI-negative) *m/z*: 611 [M – H]<sup>–</sup>, 531 [M – 2H – Br]<sup>–</sup>. Anal. (C<sub>12</sub>H<sub>5</sub>Br<sub>5</sub>O<sub>4</sub>) C, H.

**2-Methoxy-2'-nitrodiphenyl Ether (22).** To a suspension of guaiacol (280 mg, 2.3 mmol), NaH (91 mg, 2.3 mmol), and CuBr·SMe<sub>2</sub> (1.45 g, 7.03 mmol) in DMF (10 mL) was added 1-bromo-2-nitrobenzene (0.56 g, 2.3 mmol) under an argon atmosphere. The mixture was heated under refluxing conditions for 3 h and then was cooled to room temperature, diluted with EtOAc, and washed with HCl (1 M). The organic layer was washed with H<sub>2</sub>O and brine, dried (Na<sub>2</sub>SO<sub>4</sub>), and removed in vacuo. The residue was chromatographed on a silica gel column (Hex–EtOAc, 8:2) to give **22**<sup>41–42</sup> (203 mg, 36%): mp 69–70 °C; <sup>1</sup>H NMR (CDCl<sub>3</sub>): δ 7.92 (dd, *J* = 8.2, 1.5 Hz, 1H); 7.41 (td, *J* = 7.9, 1.5 Hz, 1H) 7.20 (td, *J* = 7.9, 1.5 Hz, 1H), 7.08 (m, 2H), 6.98 (m, 2H), 6.81 (dd, *J* = 8.2, 1.2 Hz, 1H), 3.76 (s, 3H); <sup>13</sup>C NMR (CDCl<sub>3</sub>): δ 151.61, 151.21, 143.13, 139.83, 133.96, 126.28, 125.51, 121.92, 121.74, 121.19, 117.96, 113.08, 55.85.

**2-Amino-2'-methoxydiphenyl Ether (23).** A suspension of **22** (850 mg, 3.47 mmol), 10% Pd/C (270 mg) in methanol (25 mL) was stirred at room temperature for 3 h under a hydrogen atmosphere. The reaction mixture was filtered throughout Celite and the Celite washed with CH<sub>2</sub>Cl<sub>2</sub>. Evaporation of the solvent in vacuo and purification of the residue by chromatography on a silica gel column (Hex–EtOAc, 7:3) afforded **23**<sup>43</sup> (700 mg, 94%): mp 60–63 °C; <sup>1</sup>H NMR (CDCl<sub>3</sub>): δ 7.06 (m, 1H), 6.98 (m, 1H), 6.94 (m, 1H), 6.87 (m, 2H), 6.79 (m, 2H), 6.68 (td, *J* = 7.3, 1.5 Hz, 1H); <sup>13</sup>C NMR (CDCl<sub>3</sub>): δ 150.32, 145.71, 143.91, 137.98, 124.05, 123.68, 120.86, 118.50 (2), 118.32, 116.09, 112.38, 55.77.

**2'-Amino-3,3',4,4',5,5'-hexabromo-2-hydroxydiphenyl Ether (24).** To a solution of **23** (213 mg, 0.99 mmol) in acetic acid (6 mL) at room temperature was added dropwise bromine (2 mL, 39.6 mmol) with stirring. The reaction mixture was heated at 95 °C for 15 h and then cooled to room temperature and concentrated in vacuo. The residue was chromatographed on a silica gel column (Hex–CH<sub>2</sub>Cl<sub>2</sub>, 3:2) to give **24** (227 mg, 34%): mp 215–216 °C; <sup>1</sup>H NMR (acetone-*d*<sub>6</sub>): δ 7.36 (s, 1H), 7.25 (s, 1H); <sup>13</sup>C NMR (acetone-*d*<sub>6</sub>): δ 147.55, 144.44, 142.78, 139.96, 123.05, 122.98, 122.39, 121.90, 115.65, 114.21, 111.76, 109.68; MS (APCI-negative) *m/z*: 674 [M – H]<sup>–</sup>, 595 [M – Br]<sup>–</sup>. Anal. (C<sub>12</sub>H<sub>5</sub>Br<sub>6</sub>NO<sub>2</sub>) C; H: calcd, 0.75; found, 0.79; N: calcd, 2.08; found, 2.09.

**2,2',4'-Trimethoxydiphenyl Ether (25).** To a suspension of guaiacol (400 mg, 3.2 mmol) in benzene (3 mL) was added NaOMe (260 mg, 4.8 mmol) under an argon atmosphere. The mixture was stirred at room temperature for 45 min. The solvent was evaporated and CuCl (318 mg, 3.2 mmol), 1-bromo-2,4-dimethoxybenzene (1.2 g, 5.4 mmol), and pyridine (4 mL) were added. The mixture was heated under refluxing for 3 h and then cooled to room temperature, diluted with EtOAc, and washed with HCl (1 M). The organic layer was successively washed with H<sub>2</sub>O and brine, dried (Na<sub>2</sub>SO<sub>4</sub>), and concentrated in vacuo. The residue was chromatographed on a silica gel column (CH<sub>2</sub>Cl<sub>2</sub>–Hex, 4:1) to give **25**<sup>44</sup> (120 mg, 14%): <sup>1</sup>H NMR (CDCl<sub>3</sub>): δ 6.96 (m, 2H), 6.88 (d, *J* = 9 Hz, 1H), 6.80 (m, 1H), 6.68 (dd, *J* = 8, 1.5 Hz, 1H), 6.56 (d, *J* = 3 Hz, 1H), 6.40 (dd, *J* = 9, 3 Hz, 1H), 3.89 (s, 3H), 3.78 (s, 3H); <sup>13</sup>C NMR (CDCl<sub>3</sub>): δ 156.74, 151.80, 149.53, 147.32, 138.59, 122.53, 120.86, 120.53, 116.29, 112.09, 103.69, 100.37, 55.81, 55.73, 55.42.

**2,2',4'-Trihydroxydiphenyl Ether (26).** To a solution of **25** (270 mg, 1.04 mmol) in 1,2-dichloroethane (3 mL) was added dropwise boron tribromide (1.56 g, 6.23 mmol) under an argon atmosphere. The mixture was stirred at room temperature for 30 h. Diethyl ether was added dropwise, and after stirring for 15 min, the mixture was diluted with EtOAc, successively washed with H<sub>2</sub>O and brine, dried (Na<sub>2</sub>SO<sub>4</sub>), and concentrated in vacuo. The residue was chromatographed on a silica gel column (CH<sub>2</sub>Cl<sub>2</sub>–EtOAc; 4:1) to give **26**<sup>44</sup> (220 mg, 97%): mp 164–166 °C. <sup>1</sup>H NMR (acetone-*d*<sub>6</sub>): δ 8.16 (br s, 3H), 6.92 (m, 2H), 6.81 (d, *J* = 9 Hz, 1H), 6.74 (m, 2H), 6.54 (d, *J* = 2.7 Hz, 1H), 6.35 (dd, *J* = 9, 2.7 Hz, 1H); <sup>13</sup>C NMR (acetone-*d*<sub>6</sub>): δ 155.54, 150.27, 148.12, 146.91, 137.22, 123.89, 122.03, 120.46, 117.34, 117.02, 107.31, 104.71.

**3,3',4,5,5'-Pentabromo-2,2',4'-trihydroxydiphenyl Ether (27).** To a solution of **26** (16 mg, 0.07 mmol) in CCl<sub>4</sub> (2 mL) was added dropwise bromine (1 mL, 19.8 mmol) with stirring. The mixture was stirred for 24 h at room temperature and then was concentrated in vacuo. The residue was chromatographed on a silica gel column (CH<sub>2</sub>Cl<sub>2</sub>–EtOAc, 95:5) to give **27** (36 mg, 80%): mp 207–209 °C. <sup>1</sup>H NMR (acetone-*d*<sub>6</sub>): δ 7.35 (s, 1H), 7.13 (s, 1H), <sup>13</sup>C NMR (acetone-*d*<sub>6</sub>): δ 150.00, 147.71, 146.67, 146.44, 136.66, 123.70, 121.39, 119.71, 114.80, 113.84, 101.64, 99.57. MS (ESI-negative) *m/z*: 612 [M – H]<sup>–</sup>, 531 [M – 2H – Br]<sup>–</sup>. Anal. (C<sub>12</sub>H<sub>5</sub>Br<sub>5</sub>O<sub>4</sub>) C; H: calcd, 0.82; found, 0.83.

**4-Fluoro-2,2'-dimethoxydiphenyl Ether (28).** Compound **28** was prepared from guaiacol (123 mg, 0.86 mmol) and 2-bromo-4-fluoroanisole (540 mg, 2.58 mmol) according to the method of preparation for **25**. The residue was chromatographed on a silica gel column (Hex–CH<sub>2</sub>Cl<sub>2</sub>, 1:3) to afford **28** (134 mg, 63%): <sup>1</sup>H NMR (CDCl<sub>3</sub>): δ 7.13 (m, 1H), 6.93 (m, 4H), 6.70 (m, 1H), 6.46 (dd, *J* = 9.5, 2.9 Hz, 1H), 3.86 (s, 3H), 3.82 (s, 3H); <sup>13</sup>C NMR (CDCl<sub>3</sub>): δ 156.81 (d, *J* = 239 Hz) 150.89, 147.30 (d, *J* = 10 Hz), 146.20 (d, *J* = 3 Hz), 144.37, 125.01, 120.93, 120.35, 112.77, 112.60, 108.48 (d, *J* = 23.2 Hz), 105.21 (d, *J* = 27.2 Hz), 56.50, 55.76.

**5-Fluoro-3,3',4,4',5'-pentabromo-2,2'-dimethoxydiphenyl Ether (29).** To a solution of **28** (72 mg, 0.29 mmol) in acetic acid (2 mL) was added dropwise bromine (0.6 mL) with stirring. The mixture was stirred at room temperature for 5 days and then was concentrated in vacuo. The residue was treated with NaOH (1 M) and extracted with CH<sub>2</sub>Cl<sub>2</sub>. The organic layer was successively washed with H<sub>2</sub>O and brine, dried (Na<sub>2</sub>SO<sub>4</sub>), and removed in vacuo. The residue was chromatographed (Hex–CH<sub>2</sub>Cl<sub>2</sub>, 85:15) to give **29** (118 mg, 64%): <sup>1</sup>H NMR (CDCl<sub>3</sub>): δ 7.21 (s, 1H), 6.71 (d, *J* = 8.8 Hz, 1H), 3.88 (s, 3H), 3.87 (s, 3H); <sup>13</sup>C NMR (CDCl<sub>3</sub>): δ 155.82 (d, *J* = 248 Hz), 149.03 (d, *J* = 10 Hz), 148.75, 148.36, 145.67 (d, *J* = 4 Hz), 123.75, 123.36, 123.16, 120.02, 108.18 (d, *J* = 24 Hz), 106.35 (d, *J* = 28 Hz), 102.16 (d, *J* = 29 Hz), 61.33, 61.24.

**5-Fluoro-3,3',4,4',5'-pentabromo-2,2'-dihydroxydiphenyl Ether (30)** To solution of **29** (120 mg, 0.21 mmol) in 1,2-dichloroethane (3 mL) was added dropwise boron tribromide (795 mg, 3.17 mmol) under an argon atmosphere. The mixture was stirred at room temperature for 30 h. Diethyl ether was added dropwise, and after stirring for 15 min, the mixture was diluted with EtOAc, washed with H<sub>2</sub>O, dried (Na<sub>2</sub>SO<sub>4</sub>), and concentrated in vacuo. The residue was chromatographed on a silica gel column (Hex–EtOAc, 3:2) to give **30** (105 mg, 82%): <sup>1</sup>H NMR (CDCl<sub>3</sub>/CD<sub>3</sub>OD): δ 7.12 (s, 1H), 6.69 (d, *J* = 8.8 Hz, 1H); <sup>13</sup>C NMR (CDCl<sub>3</sub>/CD<sub>3</sub>OD): δ 152.7 (d, *J* = 243 Hz), 145.87, 142.98, 142.85, 142.76, 123.39, 121.55, 115.57, 115.36 (d, *J* = 30 Hz), 114.11, 108.0 (d, *J* = 24 Hz), 105.34 (d, *J* = 28 Hz); MS (APCI-negative) *m/z*: 614 [M – H]<sup>–</sup>, 535 [M – Br]<sup>–</sup>. Anal. (C<sub>12</sub>H<sub>4</sub>Br<sub>5</sub>FO<sub>3</sub>) C; H: calcd, 0.66; found, 0.59.

**3,3',4,4',5,5'-Hexabromo-2,2'-dimethoxydiphenylamine (32).** To a solution of 2,2'-dimethoxyphenylamine<sup>28</sup> (200 mg, 0.87 mmol) in CCl<sub>4</sub> (4 mL) was added dropwise bromine (2.23 g, 19.95 mmol) while stirring. The mixture was stirred at room temperature for 14 h and then was concentrated in vacuo. The residue was chromatographed on a silica gel column (Hex–EtOAc, 3:1) to afford **32** (541 mg, 88%): mp 192–195 °C; <sup>1</sup>H NMR (CDCl<sub>3</sub>) δ 7.04 (s, 2H), 3.62 (s, 6H); <sup>13</sup>C NMR (CDCl<sub>3</sub>) δ 149.70, 130.67, 117.33, 117.16, 115.32, 113.52, 55.02; MS (ES-negative) *m/z*: 702 [M – H]<sup>–</sup>. Anal. (C<sub>14</sub>H<sub>9</sub>Br<sub>6</sub>NO<sub>2</sub>) C; H: calcd, 1.29; found, 1.31; N: calcd, 1.99; found, 2.07.

**3,3',4,4',5,5'-Hexabromo-2,2'-dihydroxydiphenylamine (33).** Compound **33** was prepared from **32** (100 mg, 0.14 mmol) according to the method of preparation for **26**. The residue was chromatographed on a silica gel column (Hex–EtOAc, 3:1) to give **33** (33 mg, 34%): mp > 300 °C; <sup>1</sup>H NMR (CD<sub>3</sub>OD) δ 7.08 (s, 2H), 5.56 (br s, 1H); <sup>13</sup>C NMR (CD<sub>3</sub>OD) δ 151.78, 133.46, 120.83, 119.39, 117.91, 117.16; MS (FAB-positive) *m/z*: 675 [M]<sup>+</sup>. Anal. (C<sub>12</sub>H<sub>5</sub>Br<sub>6</sub>NO<sub>2</sub>) C; H: calcd, 0.75; found, 0.80; N: calcd, 2.08; found, 2.12.

**B. Biological Methods. Production and Purification of Recombinant Human Aldose Reductase.** Recombinant

hALR2 was obtained and purified as previously described.<sup>45</sup> Insect cells of *Spodoptera frugiperda* Sf9 (Pharmlingen, 21300C) were cultured in Grace's medium (Gibco) at 27 °C without CO<sub>2</sub>. Once the stationary growing phase was reached, cultures were infected with baculovirus *Autographa californica* AcAr that has been genetically modified by the insertion of the human aldose reductase gene in its genome.<sup>46</sup> These infected cells were able to produce hALR2, which was recovered and purified from the culture medium by affinity chromatography in Matrex Gel Orange A (Amicon). After its elution with NADPH, the enzyme was stored at -20 °C in storage buffer (50 mM sodium phosphate, pH 7.0, 5 mM dithiothreitol, and 50% glycerol).

**Recombinant Human Aldose Reductase Inhibition.** The hALR2 activity assays were carried out according to a previously described method<sup>45</sup> that is based on the quantification of NADPH consumption which takes place when hALR2 catalyses the conversion of glyceraldehyde into glycerol. This assay was carried out in 96-well microtiter plates at 37 °C in 100 mM sodium phosphate buffer pH 6.2, 400 mM ammonium sulfate, 5 mU/mL of recombinant hALR2 (1 mU of activity was defined as a change in absorbance of 0.012 units per minute), and 0.1 mM NADPH. The final reaction volume was 200  $\mu$ L per well.

The compounds to be assayed were dissolved in dimethyl sulfoxide, and the corresponding solution was added to the well and preincubated for 5 min at 37 °C prior to addition of the substrate. The reaction was initiated by addition of 10 mM glyceraldehyde, and the decrease in optical density at 340 nm was monitored for 6 min at 37 °C in a microtiter plate reader (MRX-TCII, Dynex Technologies) in three intervals of 2 min each. The IC<sub>50</sub> for each test compound was determined as the compound concentration that inhibited hALR2 activity by 50%. Values are given as the mean of three experiments  $\pm$  the standard deviation.

**Intracellular Sorbitol Accumulation in Human Retinal Cells ARPE-19.** Intracellular concentrations of sorbitol in human retinal cells ARPE-19 (ATCC CRL 2302) were measured following the recommended protocol.<sup>47</sup> In brief, 10  $\times$  10<sup>6</sup> retinal human cells were cultured in 2.5 mL of Minimum Essential Medium (JRH Biosciences) supplemented with 0.5% fetal calf serum. 50 mM glucose was added to the culture medium to reproduce in vitro the typical hyperglycemia conditions of diabetes mellitus. The compounds to be assayed were dissolved in dimethyl sulfoxide, and the corresponding solution was added to the well. After an incubation of 16 h at 37 °C with 5% CO<sub>2</sub>, the accumulated sorbitol inside the cells was extracted by lysis with 8% perchloric acid and then neutralized with KOH.<sup>48</sup> Quantification of sorbitol was carried out using a colorimetric method (D-Sorbitol/xylitol, Boehringer Mannheim, 670 057). The IC<sub>50</sub> for each test compound was determined as the compound concentration that inhibited sorbitol accumulation by 50%. Values are given as the mean of three experiments.

**C. Computational Methods. Force Field Parameters.** The second-generation all-atom AMBER molecular mechanics force field was used for the enzyme, and consistent parameters for the NADP<sup>+</sup> cofactor (Supporting Information), zopolrestat, and halogenated inhibitors were derived to describe the bonded and nonbonded interactions. For each inhibitor, molecular electrostatic potentials (MEPs) were calculated from the corresponding ab initio wave functions (RHF 6-31G\*\*//3-21G\*) using Gaussian94<sup>49</sup> following full energy minimization. Partial atomic charges were then obtained by fitting each MEP to a monopole-monopole expression using the RESP methodology.<sup>50</sup> Atom types for aromatic carbon atoms in the inhibitors (CA) were taken from the AMBER database. Equilibrium bond lengths and angles involving halogen atoms were obtained from the ab initio 6-31G(d) energy-minimized structures of fluorobenzene, chlorobenzene, and bromobenzene (Table 3). Nonbonded parameters for F, Cl, and Br in these molecules were developed and tested essentially by following our previously reported procedure.<sup>51</sup> In brief, a periodic cubic box (24  $\times$  24  $\times$  24  $\text{\AA}^3$ ) containing 75 molecules of benzene was first constructed to ascertain that the standard AMBER parameters

were able to reproduce the density (0.876 g cm<sup>-3</sup>) and enthalpy of vaporization ( $\Delta H_{\text{vap}} = 8.11 \text{ kcal mol}^{-1}$ ) of this liquid at 300 K and 1 atm using a compressibility value of  $96.7 \times 10^{-6} \text{ bar}^{-1}$ .<sup>51</sup> The starting geometry was provided by the typical "herringbone" packing arrangement observed in the crystallographic structure of deuterated benzene.<sup>52</sup> Once this box was equilibrated (density =  $0.91 \pm 0.01 \text{ g cm}^{-3}$  and  $\Delta H_{\text{vap}} = 8.35 \pm 0.13 \text{ kcal mol}^{-1}$ ), the simple operation of replacing one of the hydrogen atoms in each benzene molecule by the appropriate halogen atom yielded the preequilibrated boxes of fluorobenzene, chlorobenzene, and bromobenzene. The compressibility values (in  $10^{-6} \text{ bar}^{-1}$ ) used for these solvents were, respectively, 87.3, 75.1, and 66.8. Molecular dynamics simulations were carried out at 300 K using the SANDER module in AMBER and a dielectric constant of unity. Both the temperature and the pressure were coupled to thermal and pressure baths with relaxation times of 0.2 and 0.6 ps, respectively. In a 20-ps heating phase, the temperature was gradually raised under constant volume conditions, and the velocities were reassigned at each new temperature according to a Maxwell-Boltzmann distribution. This was followed by an equilibration phase of 300 ps at 300 K, and by a 400-ps sampling period at constant pressure during which system coordinates were saved every 50 ps. All bonds involving hydrogens were constrained to their equilibrium values by means of the SHAKE algorithm, which allowed an integration time step of 2 fs to be used. A nonbonded cutoff of 10  $\text{\AA}$  was employed and the lists of nonbonded pairs were updated every 25 steps. Density values were provided directly by the SANDER module whereas  $\Delta H_{\text{vap}}$  values were calculated according to the equation:

$$\Delta H_{\text{vap}} = RT - E_{\text{inter}}$$

where  $E_{\text{inter}}$  is the interaction energy of the system, which encompasses both the electrostatic (Eele) and van der Waals (EvdW) components, divided by the number of molecules in each box. These energy values were obtained directly from the SANDER output but were corrected to eliminate contributions from intramolecular nonbonded interactions beyond the explicitly calculated 1-4. To this end an analysis of each saved snapshot was carried out with module ANAL setting the cutoff radius to zero; because of the residue-based cutoff in AMBER, the Eele and EvdW values thus obtained contain only the intramolecular nonbonded interactions, which were subtracted from the corresponding total values provided by SANDER to yield the required intermolecular components.<sup>53</sup>

**Construction and Refinement of the Enzyme-Inhibitor Complexes.** An atomic model of human ALR2 in complex with zopolrestat was built using as templates both the C $\alpha$  trace of the zopolrestat-bound human enzyme and the all-atom structure of the porcine enzyme in complex with tolrestat, both available from the Protein Data Bank (PDB entries 1mar and 1ah3, respectively). Superposition of the C $\alpha$  trace of both proteins showed that they are virtually overlapped (root-mean-square deviation = 0.45  $\text{\AA}$  for residues 2-314). In fact, there are only minimal differences in dihedral angles between both C $\alpha$  traces (Figure 2 of the Supporting Information) and the location of the NADP<sup>+</sup> atoms in both complexes is almost identical. The porcine and human ALR2 enzymes differ in 43 out of 315 amino acids: the side chains of those that are nonequivalent were replaced in porcine ALR2 with those from their human counterparts using the built-in library of conformers within Insight II.<sup>54</sup> For each "mutated" residue, the  $\chi_1$  angle was maintained and the rotamer producing the lowest steric clash was chosen. A short optimization run restraining zopolrestat, NADP<sup>+</sup>, and all C $\alpha$  atoms of the protein to their initial coordinates allowed readjustment of covalent bonds and van der Waals contacts without changing the overall conformation of the protein.

**Automated Docking Studies.** The Lamarckian genetic algorithm<sup>55</sup> implemented in AutoDock 3.0<sup>56</sup> was used to generate docked conformations of each ligand within the binding site by randomly changing torsion angles and overall orientation of the molecule. Default settings were used except

for number of runs, population size and maximum number of energy evaluations, which were fixed to 50, 100, and 250000, respectively. Rapid intra- and intermolecular energy evaluation of each configuration was achieved by having the receptor's atomic affinity potentials for carbon, oxygen, hydrogen, and halogen atoms precalculated in a three-dimensional grid with a spacing of 0.375 Å (additional maps for nitrogen and sulfur atoms were needed for zopolrestat). AMBER nonbonded parameters for halogens were transformed into suitable AutoDock 3.0 (Table 1 of the Supporting Information) using the procedure described in the manual and a linear free energy regression coefficient of 0.1485.

**Energy Refinement of the Complexes.** To include the effects of solvation explicitly, a spherical "cap" of TIP3P water molecules<sup>57</sup> was added to the complex within 28.5 Å of the center of mass of the bound inhibitor. In the solvation process, any water molecule closer than 1.0 Å to any atom of the complex was removed. A total of 1398 water molecules were thus included and restrained from leaving this spherical boundary by means of a harmonic radial potential with a force constant of 0.6 kcal mol<sup>-1</sup> Å<sup>-2</sup>. Energy refinement was accomplished in a sequential fashion. First, the positions of all hydrogen atoms were optimized using 1200 steps of steepest descent followed by conjugate gradient energy minimization until the root-mean-square value of the potential energy gradient was below 0.01 kcal mol<sup>-1</sup> Å<sup>-1</sup>. Next, the water molecules, NADP<sup>+</sup>, bound inhibitor and those protein residues within a 14 Å sphere centered on the inhibitor were allowed to move while the remaining protein residues were fixed at their starting locations although they were included in the determination of the forces. The resulting system was then optimized by using 500 steps of steepest descent energy minimization followed by conjugate gradient until the root-mean-square value of the potential energy gradient was below 0.01 kcal mol<sup>-1</sup> Å<sup>-1</sup>. The temperature was gradually raised from 100 to 298 K over 30 ps. Following 20 ps of equilibration, a 950 ps trajectory at 298 K was then simulated, and coordinates were saved every ps. All bonds involving hydrogens were constrained to their equilibrium values using SHAKE, a time step of 2 fs was employed, and the nonbonded pairs list was updated every 25 steps. The nonbonded cutoff was 13.0 Å, and a dielectric constant of unity was employed. The ANAL module of AMBER 6.0 was used for energy decomposition of the refined complexes.

**Estimation of the Electrostatic Contributions to the Free Energies of Binding: Continuum Electrostatics Calculations.** The overall electrostatic free energy change upon binding ( $\Delta G_{\text{ele}}$ ) was calculated from the total electrostatic energy of the system by running 3 consecutive calculations on an identically defined grid: one for all the atoms in the complex,  $G_{\text{ele}}^{\text{EI}}$ , one for the enzyme atoms alone,  $G_{\text{ele}}^{\text{E}}$ , and a third one for the inhibitor atoms alone,  $G_{\text{ele}}^{\text{I}}$ . In these calculations the cofactor was considered to be part of the protein. Since the grid definition is the same in the three calculations, the grid energy artifact cancels out when the electrostatic contribution to the binding free energy is expressed as the difference in energy between the bound and the unbound molecules:

$$\Delta G_{\text{ele}} = G_{\text{ele}}^{\text{EI}} - (G_{\text{ele}}^{\text{E}} + G_{\text{ele}}^{\text{I}})$$

The Poisson–Boltzmann equation was solved using a finite difference method,<sup>58</sup> as implemented in the DelPhi module of Insight II.<sup>54</sup> The atomic coordinates employed were those of the energy-refined average structure. The interior of the enzyme, the cofactor, and the inhibitor was considered as a low dielectric medium ( $\epsilon = 4$ ) whereas the surrounding solvent was treated as a high dielectric medium ( $\epsilon = 80$ ) with ionic strength of 0.145 M. The same cubic grid, which was centered on the complex and had a resolution of 0.5 Å, was used in the three cases. A minimum separation of 10 Å was left between any solute atom in the complex and the borders of the box. The solute boundaries were defined by solvent-accessible surfaces, which were calculated with a spherical probe of 1.4

Å radius. The potentials at the grid points delimiting the box were calculated analytically by treating each charged atom as a Debye–Hückel sphere.

For energy decomposition, the binding process was divided in two stages, the first one consisting in desolvating the apposing surfaces of both the ligand and the receptor, and a second one consisting in letting the charges of the two molecules interact in the presence of the surrounding solvent. The procedure has been described in detail previously.<sup>31,59,60</sup> Briefly, the cost of desolvating both the enzyme and the ligand was calculated by considering the effects on the respective electrostatic free energies of replacing the high dielectric medium of the solvent with the low dielectric medium of the other molecule in those regions that are occupied by the binding partner in the complex. To calculate the residue-based ligand–receptor interaction energies, the solvent-corrected potential generated by the charges on the ligand was computed at the positions of each of the uncharged atoms of the receptor.

**Free Energy Perturbation Calculations.** The molecular dynamics–thermodynamic integration method, as implemented in AMBER 6.0, was used to investigate the differences in binding free energy between compounds **1** and **2** and to verify the reliability of the proposed binding mode. Nonbonded intramolecular contributions were included in the evaluation of the free energy differences, as recommended.<sup>61</sup> Compound **1** and **2** were each immersed in a rectangular box containing ~700 water molecules. Following heating and equilibration for 950 ps, as described previously, the Br → H or H → Br "mutations" took place over a total of 41 "windows", each consisting of 5 ps of equilibration and 5 ps of data collection for averaging. The same mutations were performed in the cap-solvated hALR2:NADP<sup>+</sup>:**1** and hALR2:NADP<sup>+</sup>:**2** complexes under the conditions described above. The relative free energy differences were calculated as  $\Delta\Delta G_{\text{binding}} = \Delta G_{\text{binding}}(\mathbf{2}) - \Delta G_{\text{binding}}(\mathbf{1}) = \Delta G_4 - \Delta G_3$  (Scheme 7).

**Acknowledgment.** We thank the O.N.C.E. Foundation (Spain) for their interest and financial support in the Aldose Reductase Inhibitors Project. We are very much obliged to Dr. C. Nishimura (National Children's Medical Research Center, Tokyo, Japan), Dr. Ulf Ryde (Department of Theoretical Chemistry, Lund University, Sweden), and Dr. B. Bowden (James Cook University, Townsville, Australia) for kindly providing us, respectively, with the baculovirus, AMBER parameters for NADP<sup>+</sup>, and marine natural compounds **1–3**. A predoctoral fellowship to S. Manzanaro from the Spanish Ministerio de Ciencia y Tecnología (MIT-F2) is gratefully acknowledged. The authors thank Irene Palacios for technical assistance and Marta Martínez, Ada Cañedo, and Susana González for the spectroscopic studies.

**Supporting Information Available:** A table containing AutoDock parameters for the inhibitors, two figures showing van der Waals and electrostatic contributions to the binding energy of zopolrestat (Figure 1) and pairwise differences in  $\text{C}\alpha$  dihedral angles along the peptide backbone of the different complexes studied (Figure 2), and the AMBER PREP file used for NADP<sup>+</sup>. This material is available free of charge via the Internet at <http://pubs.acs.org>.

## References

- Brownlee, M. Biochemistry and Molecular Cell Biology of Diabetic Complications. *Nature* **2001**, *414*, 813–820.
- Gabbay, K. H. The Sorbitol Pathway and the Complications of Diabetes. *N. Engl. J. Med.* **1973**, *288*, 831–836.
- Kador, P. F. The Role of Aldose Reductase in the Development of Diabetic Complications. *Med. Res. Rev.* **1988**, *8*, 325–352.
- Tomlinson, D. R.; Stevens, E. J.; Diemel, L. Aldose Reductase Inhibitors and Their Potential for the Treatment of Diabetic Complications. *Trends Pharmacol. Sci.* **1994**, *15*, 293–297.
- Crabbe, M. J. C.; Goode, D. Aldose Reductase: a Window to the Treatment of Diabetic Complications? *Prog. Retin. Eye Res.* **1998**, *17*, 313–383.

- (6) Yabe-Nishimura, C. Aldose Reductase in Glucose Toxicity: a Potential Target for the Prevention of Diabetic Complications. *Pharmacol. Rev.* **1998**, *50*, 21–33.
- (7) Carper, D. A.; Wistow, G.; Nishimura, C.; Graham, C.; Watanabe, K.; Fujii, Y.; Hayashi, H.; Hayaishi, O. A Superfamily of NADPH-Dependent Reductases in Eukaryotes and Prokaryotes. *Exp. Eye Res.* **1989**, *49*, 377–388.
- (8) Costantino, L.; Rastelli, G.; Vianello, P.; Cignarella, G.; Barlocco, D. Diabetes Complications and Their Potential Prevention: Aldose Reductase Inhibition and Other Approaches. *Med. Res. Rev.* **1999**, *19*, 3–23.
- (9) Costantino, L.; Rastelli, G.; Cignarella, G.; Vianello, P.; Barlocco, D. New Aldose Reductase Inhibitors as Potential Agents for the Prevention of Long-term Diabetic Complications. *Exp. Opin. Ther. Pat.* **1997**, *7*, 843–858.
- (10) Sarges, R.; Oates, P. J. Aldose Reductase Inhibitors: Recent Developments. *Prog. Drug Res.* **1993**, *40*, 99–161.
- (11) De la Fuente, J. A.; Manzanaro, S. Aldose Reductase Inhibitors from Natural Sources. *Nat. Prod. Rep.* **2003**, *20*, 243–251.
- (12) Rondeau, J.-M.; Tete-Favier, F.; Podjarny, A.; Reymann, J. M.; Barth, P.; Biellmann, J. F.; Moras, D. Novel NADPH-binding Domain Revealed by the Crystal Structure of Aldose Reductase. *Nature (London)* **1992**, *355*, 469–472.
- (13) Urzhumtsev, A.; Tete-Favier, F.; Mitschler, A.; Barbanton, J.; Parth, P.; Urzhumtseva, L.; Biellmann, J.-F.; Podjarny, A. D.; Moras, D. A 'Specificity' Pocket Inferred from the Crystal Structures of the Complexes of Aldose Reductase with Pharmacologically Important Inhibitors Tolrestat and Sorbinil. *Structure* **1997**, *5*, 601–612.
- (14) Wilson, D. K.; Bohren, K. M.; Gabbay, K. H.; Quiocho, F. A. An Unlikely Sugar Substrate in the 1.65 Å Structure of the Human Aldose Reductase Holoenzyme Implicated in Diabetic Complications. *Science* **1992**, *257*, 81–84.
- (15) Wilson, D. K.; Tarle, I.; Petrash, J. M.; Quiocho, F. A. Refined 1.8 Å Structure of Human Aldose Reductase Complexed with the Potent Inhibitor Zopolrestat. *Proc. Natl. Acad. Sci. U.S.A.* **1993**, *90*, 9847–9851.
- (16) Warren, J. C.; Murdock, G. L.; Ma, Y.; Goodman, S. R.; Zimmer, W. E. Molecular Cloning of Testicular 20 Alpha-Hydroxysteroid Dehydrogenase: Identity with Aldose Reductase. *Biochemistry* **1993**, *32*, 1401–1406.
- (17) Várnai, P.; Warshel, A. Computer Simulation Studies of the Catalytic Mechanism of Human Aldose Reductase. *J. Am. Chem. Soc.* **2000**, *122*, 3849–3860.
- (18) Sugiyama, K.; Chen, Z.; Lee, Y. S.; Kador, P. F. Isolation of a Non-Covalent Aldose Reductase-Nucleotide-Inhibitor Complex. *Biochem. Pharmacol.* **2000**, *59*, 329–336.
- (19) Bohren, K. M.; Grimshaw, C. E. The Sorbinil Trap: a Predicted Dead-end Complex Confirms the Mechanism of Aldose Reductase Inhibition. *Biochemistry* **2000**, *39*, 9967–9974.
- (20) Rastelli, G.; Antolini, L.; Benvenuti, S.; Costantino, L. Structural Bases for the Inhibition of Aldose Reductase by Phenolic Compounds. *Bioorg. Med. Chem.* **2000**, *8*, 1151–1158.
- (21) Costantino, L.; Rastelli, G.; Gamberini, M. C.; Vinson, J. A.; Bose, P.; Iannone, A.; Staffieri, M. G.; Antolini, L.; Del Corso, A.; Mura, U.; Albasini, A. 1-Benzopyran-4-one Antioxidants as Aldose Reductase Inhibitors. *J. Med. Chem.* **1999**, *42*, 1881–1893.
- (22) Pfeifer, M. A.; Schumer, M. P.; Gelber, D. A. Aldose Reductase Inhibitors: the End of an Era or the Need for Different Trial Designs? *Diabetes* **1997**, *46 Suppl. 2*, S82–89.
- (23) Norton, R. S.; Croft, K. D.; Wells, R. J. Polybrominated Oxydiphenol Derivatives from the Sponge *Dysidea herbacea*. Structure Determination by Analysis of  $^{13}\text{C}$  Spin–Lattice Relaxation Data for Quaternary Carbons and  $^{13}\text{C}$ – $^1\text{H}$  Coupling Constants. *Tetrahedron* **1981**, *37*, 2341–2349.
- (24) Masashi, N.; Misako, I.; Yoshihiro, H.; Mamoru, E. Aldose Reductase Inhibitor from Palauan Sponges. *Tennen Yuki Kagobutsu Toronkai Koen Yoshishu* **1986**, *28*, 200–207.
- (25) Fu, X.; Schmitz, F. J.; Govindan, M.; Abbas, S. A.; Hanson, K. M.; Horton, P. A.; Crews, P.; Laney, M.; Schatzman, R. C. Enzyme Inhibitors: New and Known Polybrominated Phenols and Diphenyl Ethers from Four Indo-Pacific *Dysidea* Sponges. *J. Nat. Prod.* **1995**, *58*, 1384–1391.
- (26) Carté, B.; Faulkner, J. Polybrominated Diphenyl Ethers from *Dysidea herbacea*, *Dysidea chlorea* and *Phyllospongia foliascens*. *Tetrahedron* **1981**, *37*, 2335–2339.
- (27) Teshirogi, I.; Matsutani, S.; Shirahase, K.; Fujii, Y.; Yoshida, T.; Tanaka, K.; Ohtani, M. Synthesis and Phospholipase A<sub>2</sub> Inhibitory Activity of Thielocin B3 Derivatives. *J. Med. Chem.* **1996**, *39*, 5183–5191.
- (28) Murakami, Y.; Yokoyama, Y.; Sasakura, C.; Tamagawa, M. An Efficient Synthesis of 1,1'-Disubstituted Hydrazines. *Chem. Pharm. Bull.* **1983**, *31*, 423–428.
- (29) Nakai, N.; Fujii, Y.; Kobashi, K.; Nomura, K. Aldose Reductase Inhibitors: Flavonoids, Alkaloids, Acetophenones, Benzophenones, and Spirohydantoin of Chroman. *Arch. Biochem. Biophys.* **1985**, *239*, 491–496.
- (30) Cornell, W. D.; Cieplak, P.; Bayly, C. I.; Gould, I. R.; Merz, K. M.; Ferguson, D. M.; Spellmeyer, D. C.; Fox, T.; Caldwell, J. W.; Kollman, P. A. A Second Generation Force Field for the Simulation of Proteins, Nucleic Acids, and Organic Molecules. *J. Am. Chem. Soc.* **1995**, *117*, 5179–5197.
- (31) Kmunicek, J.; Luengo, S.; Gago, F.; Ramirez Ortiz, A.; Wade, R.; Damborsky, J. Comparative Binding Energy (COMBINE) Analysis of the Substrate Specificity of Haloalkane Dehalogenase from *Xanthobacter autotrophicus* GJ10. *Biochemistry* **2001**, *40*, 8905–8917.
- (32) Kinoshita, T.; Miyake, H.; Fujii, T.; Takakura, S.; Goto, T. The structure of human recombinant aldose reductase complexed with the potent inhibitor zenarestat. *Acta Crystallogr. D Biol. Crystallogr.* **2002**, *58*, 622–626.
- (33) Hansch, C.; Leo, A. In *Substituent Constants for Correlation Analysis in Chemistry and Biology*; John Wiley: New York, 1979.
- (34) Lobaton, E.; Rodriguez-Barrios, F.; Gago, F.; Pérez-Pérez, M. J.; De Clercq, E.; Balzarini, J.; Camarasa, M. J.; Velázquez, S. Synthesis of 3''-substituted TSAO derivatives with anti-HIV-1 and anti-HIV-2 activity through an efficient palladium-catalyzed cross-coupling approach. *J. Med. Chem.* **2002**, *45*, 3934–3945.
- (35) Kime, D. E.; Norymberski, J. K. Synthesis of Fully Aromatic Cyclic Polyethers. *J. Chem. Soc., Perkin Trans. 1* **1977**, 1048–1052.
- (36) Deng, G.; James, T. D.; Shinkai, S. Allosteric Interactions of Metal Ions with Saccharides in a Crowned Diboronic Acid. *J. Am. Chem. Soc.* **1994**, *116*, 4567–4572.
- (37) McOmie, J. F. W.; West, D. E. *Organic Syntheses*; Wiley: New York, 1973; Collect. Vol. V, p 412.
- (38) Rao, A. V. R.; Gurjar, M. K.; Kaiwar, V.; Khare, V. B. An Expedient Approach to the Diphenyl Ether Cross-linked Amino Acids of Glycopeptide Antibiotics. *Tetrahedron Lett.* **1993**, *34*, 1661–1664.
- (39) Ugnade, H. E.; Zilch, K. T. Phenoxyquinones II. The Diphenoxyquinones. *J. Org. Chem.* **1951**, *16*, 64–69.
- (40) Allard, A.-S.; Remberger, M.; Neilson, A. H. Bacterial O-Methylation of Halogen-Substituted Phenols. *Appl. Environ. Microbiol.* **1987**, *53*, 839–845.
- (41) Scarborough, H. A.; Sweeten, J. L. Substitution Products of 2'-Nitro- and 2':4'-Dinitro-2-methoxy-diphenyl Ethers. *J. Chem. Soc.* **1934**, 867–869.
- (42) Cullinane, N. M.; Davey, H. G.; Padfield, H. J. H. Investigations in the Diphenylene Oxide Series. Part IV. *J. Chem. Soc.* **1934**, 716–719.
- (43) Olmsted, M. P.; Craig, P. N.; Lafferty, J. J.; Pavloff, A. M.; Zirkle, C. L. Analogues of Phenothiazines. II. Phenoxazine and Phenoselenazine Analogues of Phenothiazine Drugs. *J. Org. Chem.* **1961**, *26*, 1901–1907.
- (44) Glombitza, K. W.; Woelwer-Rieck, U. Antibiotics from Algae. 38. Base-catalyzed Reactions of Multiple Hydroxylated Diphenyl Ethers. *Liebigs Annalen der Chemie* **1988**, *3*, 261–265.
- (45) Nishimura, C.; Yamaoka, T.; Mizutani, M.; Yamashita, K.; Akera, T.; Tanimoto, T. Purification and Characterization of the Recombinant Human Aldose Reductase Expressed in Baculovirus System. *Biochim. Biophys. Acta.* **1991**, *1078*, 171–178.
- (46) Nishimura, C.; Matsuura, Y.; Kokai, Y.; Akera, T.; Carper, D.; Morjana, N.; Lyons, C.; Flynn, T. G. Cloning and Expression of Human Aldose Reductase. *J. Biol. Chem.* **1990**, *265*, 9788–9792.
- (47) Rink, H.; Baumstark-Khan, C. Cell Culture Methods. In *Manual of Oculotoxicity*; Hockwin, O., Green, K., Rubin, L. F., Eds.; Gustav Fischer Verlag: Stuttgart, Germany, 1992; pp 389–401.
- (48) Yaginuma, S.; Asahi, A.; Takada, M.; Hayashi, M.; Tsujino, M.; Mizuno, K. Aldostatin, a New Aldose Reductase Inhibitor. In *Novel Microbial Products for Medicine and Agriculture*; Demain, A. L., Somkuti, G. A., Hunter-Cevera, J. C., Rossmore, H. W., Eds.; Society for Industrial Microbiology; Elsevier Science Ltd: New York, 1989; pp 127–133.
- (49) Gaussian 94, Revision E.1, Frisch, M. J.; Trucks, G. W.; Schlegel, H. B.; Gill, P. M. W.; Johnson, B. G.; Robb, M. A.; Cheeseman, J. R.; Keith, T.; Petersson, G. A.; Montgomery, J. A.; Raghavachari, K.; Al-Laham, M. A.; Zakrzewski, V. G.; Ortiz, J. V.; Foresman, J. B.; Cioslowski, J.; Stefanov, B. B.; Nanayakkara, A.; Challacombe, M.; Peng, C. Y.; Ayala, P. Y.; Chen, W.; Wong, M. W.; Andres, J. L.; Replogle, E. S.; Gomperts, R.; Martin, R. L.; Fox, D. J.; Binkley, J. S.; Defrees, D. J.; Baker, J.; Stewart, J. P.; Head-Gordon, M.; Gonzalez, C. and Pople, J. A., Gaussian, Inc., Pittsburgh, PA, 1995.
- (50) Bayly, C. I.; Cieplak, P.; Cornell, W. D.; Kollman, P. A. A Well-Behaved Electrostatic Potential Based Method Using Charge Restraints for Deriving Atomic Charges: the RESP Model. *J. Phys. Chem.* **1993**, *97*, 10269–10280.
- (51) Lide, D. R. *CRC Handbook of Chemistry and Physics*; CRC Press: Boca Raton, FL, 1997.
- (52) Jeffrey, G. A.; Ruble, J. R.; McMullan, R. K.; Pople, J. A. The Crystal Structure of Deuterated Benzene. *Proc. R. Soc. London A* **1987**, *414*, 47–57.

- (53) Fox, T.; Kollman, P. A. Application of the RESP Methodology in the Parametrization of Organic Solvents. *J. Phys. Chem. B* **1998**, *102*, 8070–8079.
- (54) Insight II, version 98.0, 1998. Molecular Simulations Inc. 9685 Scranton Road, San Diego, CA 92121-2777.
- (55) Morris, G. M.; Goodsell, D. S.; Halliday, R. S.; Huey, R.; Hart, W. E.; Belew, R. K.; Olson, A. J. Automated Docking Using a Lamarckian Genetic Algorithm and an Empirical Binding Free Energy Function. *J. Comput. Chem.* **1998**, *19*, 1639–1662.
- (56) Morris, G. M.; Goodsell, D. S.; Huey, R.; Hart, W. E.; Halliday, S.; Belew, R.; Olson, A. J. AutoDock: Automated Docking of Flexible Ligands to Receptors, Version 3.0; The Scripps Research Institute: La Jolla, CA, 1999.
- (57) Jorgensen, W. L.; Chandrasekhar, J.; Madura, J. D.; Impey, R. W.; Klein, M. L. Comparison of Simple Potential Functions for Simulating Liquid Water. *J. Chem. Phys.* **1983**, *79*, 926–935.
- (58) Gilson, M. K.; Sharp, K. A.; Honig, B. H. Calculating the Electrostatic Potential of Molecules in Solution: Method and Error Assessment. *J. Comput. Chem.* **1987**, *9*, 327–335.
- (59) Pérez, C.; Ortiz, A. R.; Pastor, M.; Gago, F. Comparative Binding Energy Analysis of HIV-1 Protease Inhibitors: Incorporation of Solvent Effects and Validation as a Powerful Tool in Receptor-Based Drug Design. *J. Med. Chem.* **1998**, *41*, 836–852.
- (60) Cuevas, C.; Pastor, M.; Pérez, C.; Gago, F. Comparative Binding Energy (COMBINE) Analysis of Human Neutrophil Elastase Inhibition by Pyridone-containing Trifluoromethylketones. *Comb. Chem. High Throughput Screen.* **2001**, *4*, 627–642.
- (61) Pearlmann, D. A. Determining the Contributions of Constraints in Free Energy Calculations: Development, Characterization, and Recommendations. *J. Chem. Phys.* **1993**, *98*, 8946–8957.

JM030957N